Dynamics of bubble-bubble interactions experiencing viscoelastic drag

Ekaterina Zilonova*

*Department of Engineering Science and Ocean Engineering, National Taiwan University,
No. 1, Sec. 4, Roosevelt Road, Taipei 10617, Taiwan, Republic of China*

Maxim Solovchuk†

*Department of Engineering Science and Ocean Engineering, National Taiwan University,
No. 1, Sec. 4, Roosevelt Road, Taipei 10617, Taiwan, Republic of China
and Institute of Biomedical Engineering and Nanomedicine, National Health Research Institutes,
No. 35, Keyan Road, Zhunan 35053, Taiwan, Republic of China*

T. W. H. Sheu‡

*Department of Engineering Science and Ocean Engineering, National Taiwan University,
No. 1, Sec. 4, Roosevelt Road, Taipei 10617, Taiwan, Republic of China;
Center of Advanced Study in Theoretical Science (CASTS), National Taiwan University, Taiwan 106, Republic of China;
and Department of Mathematics, National Taiwan University, Taipei 10617, Taiwan, Republic of China*

The subject of the present theoretical study is the dynamics of bubble-bubble interactions in a viscoelastic medium. First, new equations for calculating the viscoelastic drag exerted on bubbles during their translational motion in a viscoelastic medium are derived. The drag equations are incorporated in the bubble-bubble interaction model in which, thereby, both the translational and radial motions of the bubbles are affected by the viscoelastic features of the medium. Second, the derived equations are applied to investigate how the viscoelastic properties of the medium can affect the dynamics of multiple bubbles, as well as how the bubbles can affect each other. It was discovered that the bubble-bubble interaction can significantly influence the dynamics of a single bubble. As the distance between the bubbles increases, their effect on each other decreases, and at a distance of several millimeters, this effect can be neglected. Moreover, it was concluded that with increasing elasticity and viscosity of the medium, as well with decreasing relaxation time, the effects of other bubbles on the current bubble's radial motion can become negligible. The translational motion of the bubbles was investigated for different viscoelastic models. The elasticity resists the motion of bubbles in space, resulting in a dynamical steady state of the distance between the bubbles at high elasticity values. The relaxation time of the medium was also found to be important in terms of the bubbles' translational movement.

I. INTRODUCTION

Extensive work has been performed to study cavitation in Newtonian fluids, particularly in water. Comparatively fewer investigations have been dedicated to studying cavitation in non-Newtonian fluids, namely, in viscoelastic media. However, due to the rapidly emerging biomedical applications, interest in the motion of bubbles in viscoelastic media has recently increased [1–8]. A detailed review of those biomedical applications in which cavitation plays an important role is given in Ref. [9]. Applications include tumor ablation procedures [10,11], ultrasound contrast agents for biomedical imaging [12,13], drug and gene delivery [14–17], sonothrombolysis [18,19], dentistry applications using ultrasonically vibrating probes [20,21], and cataract surgery utilizing ultrasound phacoemulsification [22]. Note that in the aforementioned therapies, the medium surrounding the bubbles is tissue fluid, blood, or saliva that display certain viscoelastic behavior. Therefore, it is essential to take the viscoelastic features of the medium surrounding the bubbles into account in the simulations of these treatments (the current study will be focused on media represented by blood and tissue fluid).

In the majority of ultrasound applications of cavitation described above, multiple bubbles or even a bubble cloud are generally present. Thus, the dynamics of multiple bubbles, including their interaction, in viscoelastic media should also be investigated. A significant contribution has been made by Doinikov [23–27] to the understanding of the translational motion of bubbles and their interaction in Newtonian fluids. Two theoretical descriptions of the translational motion of bubbles in an acoustic field exist [25]. The first description uses Newton's second law for the forces experienced by bubbles, which might include primary and secondary Bjerknes forces, added mass force, viscous drag, buoyancy force, and gravity [28–31]. The major drawback of this approach is that it

*zilorina@mail.ru
†Corresponding author: solovchuk@gmail.com
‡Corresponding author: twhsheu@ntu.edu.tw

utilizes time-averaged bubble behavior. The second approach to calculate the translational motion of bubbles is to couple bubble dynamics equations with translational motion equations [23]. This approach is able to calculate instantaneous translational motion of bubbles and is employed in the current paper. Additionally, this approach is deemed to be applicable to strong acoustic fields [25].

The bubble-bubble interaction model employed by Doinikov [23] does not simulate the viscoelastic properties of the medium surrounding the bubbles. To be able to describe bubble-bubble interactions in the biomedical applications mentioned above, the viscoelastic properties of the surrounding biological fluid should be taken into account for both the translational and radial motions of the bubbles.

The radial motion of a bubble is well known to be affected by the viscoelasticity of the surrounding medium [32–36]. Therefore, the cavitation model should be coupled with a viscoelastic model that represents the surrounding medium (as was done in the present authors' previous studies for the Gilmore-Akulichev-Zener model [34,37]). However, in the current paper, the coupling equations are modified. Moreover, the Keller-Miksis cavitation model in Ref. [23] is replaced by the Gilmore-Akulichev cavitation model [38], which is suitable for simulating the bubble dynamics under an acoustic pulse of high amplitude. The Keller-Miksis model might exceed its applicability range at high ultrasound intensities [34].

Regarding the translational motion of bubbles, the viscous drag force should be substituted with the viscoelastic drag force. Until now, for simulating the translational motion of bubbles in fluids, only viscous drag has been used (typically in the Levich form [39]). In the current paper, equations for the viscoelastic drag were derived because important properties, such as elasticity and relaxation time, might affect the motion

of bubbles in space. The drag derivation is based on the approach described in Ref. [40]. In Ref. [40], however, the derivation was performed for a single bubble of constant volume. Conversely, in the present paper, the drag equations are rederived for an oscillating bubble. Then, these equations are used for the multiple bubble model.

In the present research, equations for calculating the viscoelastic drag experienced by bubbles moving in a viscoelastic fluid are presented. Additionally, a new model capable of describing bubble-bubble interactions under an ultrasound pulse of high amplitude in a viscoelastic medium is proposed. Then, the motion of bubbles in space is studied with respect to the viscoelastic features of the surrounding medium.

II. FORMULATION

A. Bubble-bubble interaction

To describe bubble-bubble interactions, the model developed in Ref. [23] is modified in the current section. The model in Ref. [23] describes the translational motion of a bubble pair in an acoustic field and employs the Keller-Miksis cavitation model. In the current research, replacing the Keller-Miksis model with the Gilmore-Akulichev cavitation model is proposed [38]. This replacement is performed to be able to describe bubble dynamics when subjected to a driving pulse of high amplitude. The applicability range of the Gilmore-Akulichev model is larger than that of the Keller-Miksis model [34]. The Gilmore-Akulichev model can be applied for the high Mach number case that occurs at the moment of bubble collapse.

The scheme of the model is shown in Fig. 1. The equations that were proposed to describe two bubbles are written as follows:

$$R_i \ddot{R}_i \left(1 - \frac{\dot{R}_i}{C_i} \right) + \frac{3}{2} \dot{R}_i^2 \left(1 - \frac{\dot{R}_i}{3C_i} \right) - \left(1 + \frac{\dot{R}_i}{C_i} \right) \left(H_i - \frac{\tau_{rr}^{(i)}|_R}{\rho_t} + \frac{3q_i}{\rho_t} \right) - \frac{R_i}{C_i} \left[\dot{H}_i \left(1 - \frac{\dot{R}_i}{C_i} \right) - \frac{1}{\rho_t} \frac{d}{dt} \tau_{rr}^{(i)}|_R + \frac{1}{\rho_t} \frac{d}{dt} (3q_i) \right]$$

$$= \frac{\dot{x}_i^2}{4} - \frac{R_j^2 \ddot{R}_j + 2R_j \dot{R}_j^2}{d} - (-1)^i \frac{R_j^2 (\dot{x}_i \dot{R}_j + R_j \ddot{x}_j + 5\dot{R}_j \dot{x}_j)}{2d^2} - \frac{R_j^3 \dot{x}_j (\dot{x}_i + 2\dot{x}_j)}{2d^3}, \tag{1}$$

$$\frac{R_i \ddot{x}_i}{3} + \dot{R}_i \dot{x}_i - \frac{(-1)^i}{d^2} \frac{d}{dt} \left(R_i R_j^2 \dot{R}_j \right) - \frac{R_j^2}{d^3} (R_i R_j \ddot{x}_j + R_j \dot{R}_i \dot{x}_j + 5R_i \dot{R}_j \dot{x}_j) = \frac{F_{\text{ex}}^{(i)}}{2\pi \rho_t R_i^2}, \tag{2}$$

$$H_i = \frac{1}{\rho_t} \frac{n}{n-1} (p_0 + p(t) + B) \left\{ \left[\frac{\left(p_{\text{in}}^{(i)} - \frac{2S}{R_i} + \tau_{rr}^{(i)}|_R \right) + B}{p_0 + p(t) + B} \right]^{\frac{n-1}{n}} - 1 \right\}, \tag{3}$$

$$C_i = c_\infty \left[\frac{\left(p_{\text{in}}^{(i)} - \frac{2S}{R_i} + \tau_{rr}^{(i)}|_R \right) + B}{p_0 + p(t) + B} \right]^{\frac{n-1}{2n}}. \tag{4}$$

In the above equations, $R_i(t)$ and $R_j(t)$ are the radii of the ith and the jth bubble, and $x_i(t)$ and $x_j(t)$ are the positions of the centers of the ith and the jth bubble. The indexes i and j are interchangeable and they stand for the bubbles' numbers (i.e., {1, 2} or {2, 1}). $d(t) = |x_j(t) - x_i(t)|$ denotes the distance between the bubble centers. H_i is the ith bubble enthalpy, C_i is the local speed of sound at the bubble wall, c_∞ is the speed of sound, ρ_t is the density of the surrounding

medium, $\tau_{rr}^{(i)}$ is the stress in a motion in the r direction of the ith bubble, B and n are specific constants for the surrounding medium, p_0 is the static background pressure, $p(t)$ is the varying driving sound field, $p_{\text{in}}^{(i)}$ is the pressure inside the ith bubble, S is the surface tension, and $R_0^{(i)}$ is the initial radius of the ith bubble. The variable q_i is equal to $q_i = \int_{R_i}^\infty \frac{\tau_{rr}^{(i)}(r,t)}{r} dr$. This variable was introduced to be able to couple the cavitation model with the viscoelastic models.
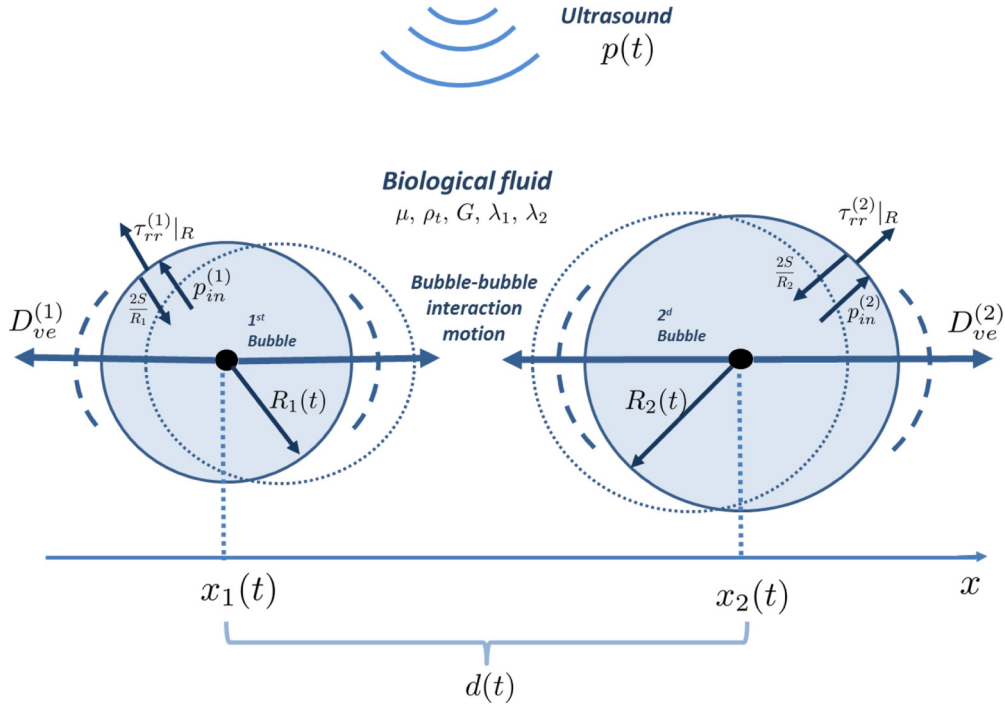
FIG. 1. Schematic of the bubble-bubble interaction model. Two bubbles with radii $R_1(t)$ and $R_2(t)$ and center positions $x_1(t)$ and $x_2(t)$ are attracted or repelled from each other in a biological viscoelastic fluid. The biological fluid is exposed to an ultrasound driving pulse $p(t)$. The bubbles are experiencing bubble-bubble interaction forces and viscoelastic drag $D_{\text{ve}}^{(i)}$, $i = \{1, 2\}$.

$F_{\text{ex}}^{(i)}$ denote instantaneous external forces acting on the bubble, such as an acoustic force that moves bubbles to pressure nodes or antinodes (can be referred to as a primary Bjerknes force) and viscous (viscoelastic) drag.

In the previous paper of the present authors [34], it was shown that, for high ultrasound frequencies and correspondingly very small periods of the wave (10^{-6} s in the current research), even adiabatic equations of state are quite a robust approximation. Thus, in the present research, the pressures inside the bubbles are assumed to follow adiabatic equations of state [41,42], namely,

$$p_{\text{in}}^{(i)} = \left(p_0 + \frac{2S}{R_0^{(i)}} \right) \left(\frac{R_0^{(i)}}{R_i} \right)^{3\gamma}. \tag{5}$$

However, for a wider range of parameters, the current model can be extended by modeling the pressure inside the bubble as a function of the bubbles' interior temperature and vapor mass transfer through the bubbles' surface [37,43].

Only linear wave propagation will be considered in this paper. The harmonic driving pulse is known to be a fair approximation of the real ultrasound pulse in terms of the bubble dynamics. Therefore, it is frequently used in simulations of the cavitation occurring in the ultrasound acoustic field [32,33,44,45]. Although nonlinear wave propagation effects can easily be added [46,47]. The ultrasound signal is $p(t) = A \sin(2\pi f t)$, where A is the pulse amplitude and f is the frequency.

In the system Eqs. (1)–(4), radial pulsations of the bubbles are represented by Eq. (1) with two extra equations for the enthalpy and local speed of sound given in Eqs. (3) and (4), respectively. The terms on the right-hand side of Eq. (1)

have been added to the traditional Gilmore-Akulichev model to take bubble-bubble interactions into account. The translational motion of the bubbles is described by Eq. (2). The second term in Eq. (2) is the contribution of the added mass force, which appears during the accelerated motion of the object in the liquid. The third and fourth terms in Eq. (2) take bubble-bubble interactions into account. In the current paper, the drag force is the only external force ($F_{\text{ex}}^{(i)} = -D_{\text{ve}}^{(i)}$). The drag equations will be derived in Sec. II C. Since the aim of this study is to understand the motion of bubbles in a viscoelastic medium, the acoustic radiation force $F_{\text{ac}} = -\frac{4\pi}{3} R^3 \nabla p(x, t)$ acting on bubbles (the primary Bjerknes force) is neglected in the current study (under the assumption that there is no phase difference in ultrasonic pressures acting on both bubbles, and $p = p(t)$ in the present one-dimensional model). This force should be taken into account in the three-dimensional extension of the current model [24] and will be studied elsewhere.

The cavitation models, such as Rayleigh-Plesset, Keller-Miksis, Herring-Trilling, and Gilmore-Akulichev, have a limitation because of the assumption of spherical symmetry. However, there are different approaches in which a bubble will be able to display an asymmetrical shape deformation. The studies dedicated to a nonspherical bubble's translational motion in a non-Newtonian fluid can be found in Refs. [48–50].

B. Viscoelastic models

Previously, bubble-bubble interactions have been considered in a viscous medium [23]. However, due to the rapid emergence of biomedical applications, there is a need to understand bubbles' interactions in viscoelastic media. Therefore, in the present section, the modified bubble-bubble interaction model [Eqs. (1)–(4)] will be coupled with different

TABLE I. Viscoelastic models.

Viscoelastic model	Counting for	Differential equation	Relaxation modulus function $E(t)$	Assumptions for Eqs. (8) and (9)
Newton model	Viscosity	$\tau_{rr} = 2\mu\dot{\gamma}_{rr}$	$\mu\delta(t)$	$\lambda_1 = 0, G = 0,$ $\lambda_2 = 0$
Maxwell model	Viscosity and relaxation time	$\tau_{rr} + \lambda_1\dot{\tau}_{rr} = 2\mu\dot{\gamma}_{rr}$	$\frac{\mu}{\lambda_1}e^{-\frac{t}{\lambda_1}}$	$G = 0, \lambda_2 = 0$
Kelvin-Voigt model	Viscosity and elasticity	$\tau_{rr} = 2G\gamma_{rr} + 2\mu\dot{\gamma}_{rr}$	$G + \mu\delta(t)$	$\lambda_1 = 0, \lambda_2 = 0$
Zener model	Viscosity, relaxation time and elasticity	$\tau_{rr} + \lambda_1\dot{\tau}_{rr} = 2G\gamma_{rr} + 2\mu\dot{\gamma}_{rr}$	$G + (\frac{\mu}{\lambda_1} - G)e^{-\frac{t}{\lambda_1}}$	$\lambda_2 = 0, \lambda_1 < \mu/G$
Jeffreys model	Viscosity, relaxation time and retardation time	$\tau_{rr} + \lambda_1\dot{\tau}_{rr} = 2\mu\dot{\gamma}_{rr} + 2\mu\lambda_2\ddot{\gamma}_{rr}$	$\frac{\mu\lambda_2}{\lambda_1}\delta(t) + (\frac{\mu}{\lambda_1} - \frac{\mu\lambda_2}{\lambda_1^2})e^{-\frac{t}{\lambda_1}}$	$G = 0, \lambda_1 > \lambda_2$

viscoelastic models. For this purpose, it is necessary to provide the equations for the stress τ_{rr} and the additional variable $q(t)$. In the following, λ_1 is the relaxation time of the surrounding medium, G is the elasticity of the surrounding medium, μ is the viscosity of the surrounding medium, and λ_2 is the retardation time of the surrounding medium.

In the current research, coupling of the bubble-bubble interaction with the following models is considered: Newton viscous model and Maxwell, Kelvin-Voigt, Zener, and Jeffreys viscoelastic models. The differences between these models are summarized in Table I.

The general equation that describes these viscoelastic models can be written as

$$\tau_{rr} + \lambda_1\frac{d\tau_{rr}}{dt} = 2G\gamma_{rr} + 2\mu\frac{d\gamma_{rr}}{dt} + 2\mu\lambda_2\frac{d^2\gamma_{rr}}{dt^2}, \quad (6)$$

where γ_{rr} is the strain and $\dot{\gamma}_{rr}$ is the strain rate. For both compressible and incompressible cases, the strain rate near the bubble surface is equal to $\dot{\gamma}_{rr} = -2\frac{R^2\dot{R}}{r^3}$ (derived from a purely radial solution of the continuity equation while neglecting terms on the order of c^{-2}, [32]). The strain is thus $\gamma_{rr} = -\frac{2}{3r^3}(R^3 - R_0^3)$, whereas $\ddot{\gamma}_{rr} = -\frac{2}{r^3}(2R\dot{R}^2 + \ddot{R}R^2)$.

The variable $q = \int_R^\infty \frac{\tau_{rr}}{r}dr$ is used. Dividing Eq. (6) by r and integrating the resulting equation from R to ∞, one can

obtain

$$q + \lambda_1\dot{q} + \lambda_1\frac{\dot{R}\tau_{rr}|_R}{R} = \frac{1}{3}\left[-\frac{4G}{3R^3}(R^3 - R_0^3) - 4\mu\frac{\dot{R}}{R}\right.$$
$$\left. - 4\mu\lambda_2\left(2\frac{\dot{R}^2}{R^2} + \frac{\ddot{R}}{R}\right)\right]. \quad (7)$$

If the viscoelastic model does not account for the relaxation time λ_1 (i.e., Newton or Kelvin-Voigt models), then the stress τ_{rr} can be calculated directly from Eq. (6), whereas the variable q in Eqs. (1)–(4) can be obtained from Eq. (7).

In previous investigations using Maxwell family models [34,35,37,51], the next step was to calculate Eq. (7) at $r = R$ to obtain an ODE equation for the variable $\tau_{rr}|_{r=R}$. However, this approach incorrectly assumes the equality of the derivatives $\frac{d\tau_{rr}|_{r=R}}{dt}$ and $\frac{d\tau_{rr}}{dt}|_{r=R}$, as noted in Ref. [33]. Nevertheless, the coupling equations proposed in Ref. [33] for the Keller-Miksis cavitation model are not suitable for the current Gilmore-Akulichev cavitation model. Therefore, in the present paper, a new, corrected equation for $\tau_{rr}|_{r=R}$ that can be coupled with the employed cavitation model is proposed. The derivation is presented in Appendix A.

As a result of the derivation, the equation for the additional variable q_i and the corrected equation for the stress $\tau_{rr}^{(i)}|_R$ that should be coupled with Eqs. (1)–(4) are as follows:

$$q_i + \lambda_1\dot{q}_i + \lambda_1\frac{\dot{R}_i\tau_{rr}^{(i)}|_R}{R_i} = \frac{1}{3}\left\{-\frac{4G}{3R_i^3}\left[R_i^3 - (R_0^{(i)})^3\right] - 4\mu\frac{\dot{R}_i}{R_i} - 4\mu\lambda_2\left(2\frac{\dot{R}_i^2}{R_i^2} + \frac{\ddot{R}_i}{R_i}\right)\right\}, \quad i = \{1, 2\}, \quad (8)$$

$$\tau_{rr}^{(i)}|_R\left(1 + 3\lambda_1\frac{\dot{R}_i}{R_i}\right) + \lambda_1\frac{d\tau_{rr}^{(i)}|_R}{dt} = -\frac{4G}{3}\left[1 - \frac{(R_0^{(i)})^3}{R_i^3}\right] - 4\mu\frac{\dot{R}_i}{R_i} - 4\mu\lambda_2\left(2\frac{\dot{R}_i^2}{R_i^2} + \frac{\ddot{R}_i}{R_i}\right), \quad i = \{1, 2\}. \quad (9)$$

Equations (8) and (9) represent the general equations that can be reduced to the Newton, Maxwell, Kelvin-Voigt, Zener, and Jeffreys models by setting certain parameters to zero (Table I).

C. Viscoelastic drag

To date, bubble-bubble interactions have been studied in a fluid medium by different authors [23–25,52–54]. Therefore,

the viscous drag was typically used in the Levich form [39]:

$$F_D = 12\pi\mu R_B U(t). \quad (10)$$

In the above equation, F_D is the drag force, $U(t)$ is the translational velocity of the moving bubble, and R_B is the radius of the bubble. Initially, this drag was derived for a bubble with an unchanged radius at the high Reynolds limit [55].

Equation (10), which corresponds to the Levich drag, simulates the drag experienced by a bubble in the viscous fluid.

It would be interesting to determine whether the viscoelastic properties of the surrounding medium will change the drag formulation. Additionally, bubbles in Sec. II A are known to be in an oscillating motion. Therefore, the unsteady drag on bubbles of variable radii in a viscoelastic fluid is an object of interest. In the current section, to achieve the above goal, the drag for a constant-volume sphere in the viscoelastic medium presented in Ref. [40] is generalized for a bubble of nonconstant volume. The generalization is performed through the use of a cell model (as done for a Newtonian fluid in Ref. [56]). In the present investigation, the obtained drag equations are presented for different viscoelastic models. The derived viscoelastic drag equations will then be coupled with the bubble-bubble interaction model.

The derivation of the drag using the cell model can be found in Appendix B. The resulting obtained equation is written as follows:

$$F_D = \frac{2\pi}{3}\rho R_B^3 \dot{U} + 2\pi \rho U \dot{R}_B R_B^2$$
$$+ 12\pi R_B \int_{-\infty}^{t} E(t - t_1) U(t_1) dt_1, \quad (11)$$

where $E(t - t_1)$ is a relaxation modulus function.

Equation (11) represents the obtained drag, which consists of three parts. The first two terms are contributed by the added-mass force given by the acceleration of the bubble's translational motion and the rate of change of the bubble radius (which was already presented in Refs. [40,56–59]). The third term is the viscoelastic drag, which is dependent on the instantaneous values of the velocity and radius of the bubble. However, note that the first two terms in Eq. (11) are already included on the left-hand side of Eq. (2). Therefore, external forces $F_{ex}^{(1)}$ and $F_{ex}^{(2)}$ in Eq. (2) should be equal only to the viscoelastic part of the drag, i.e., the third term in Eq. (11). It can be written as follows (with the assumption that the fluid is at the rest state at $t = 0$):

$$F_{ex}^{(i)} = -D_{ve}^{(i)} = -12\pi R_i \int_{0}^{t} E(t - t_1) U_i(t_1) dt_1, \quad i = \{1, 2\}.$$
$$(12)$$

For the bubble in the Newtonian fluid [$E(t) = \mu\delta(t)$], Eq. (12) reduces to the well-known Levich viscous drag (Eq. (10) [39,60,61]).

The medium surrounding the bubble can be represented by various viscoelastic models that model different biological fluids. The viscoelastic part of the drag D_{ve} will be calculated for different viscoelastic models described in Sec. II B and summarized in Table I.

1. Newton and Kelvin-Voigt drags

For the calculation of drags corresponding to the Newton and Kelvin-Voigt models (i.e., models where $\lambda_1 = 0$), the relaxation modulus function can be written as $E(t) = G + \mu\delta(t)$ (Table I). Therefore, the viscoelastic drag can be calculated as follows using Eq. (12):

$$D_{ve} = 12\pi R \int_{0}^{t} [G + \mu\delta(t - t_1)] U(t_1) dt_1$$
$$= 12\pi R G[x(t) - x_0] + 12\pi R \mu U(t)[2\theta(t) - 1]. \quad (13)$$

In the above equation, $\theta(t)$ is a Heaviside function. At $t = 0$, the viscoelastic drag is equal to zero.

Hence, the drag forces for each bubble are defined as follows for $t > 0$:

$$D_{ve}^{(i)} = 12\pi R_i [\mu \dot{x}_i + G(x_i - x_0^{(i)})], \quad i = \{1, 2\}, \quad (14)$$

where $x_0^{(1)}$ and $x_0^{(2)}$ are the initial positions of the bubbles' centers. By setting certain viscoelastic parameters equal to zero (Table I), Eq. (14) can be reduced to Newton and Kelvin-Voigt drags.

2. Maxwell, Zener, and Jeffreys viscoelastic drags

For Maxwell, Zener, and Jeffreys viscoelastic models (i.e., models where $\lambda_1 \neq 0$), the relaxation modulus function can be written as $E(t) = G + \frac{\mu\lambda_2}{\lambda_1}\delta(t) + (\frac{\mu}{\lambda_1} - \frac{\mu\lambda_2}{\lambda_1^2} - G)e^{-\frac{t}{\lambda_1}}$. The corresponding viscoelastic drag force derivation is presented in Appendix C.

Consequently, Eqs. (1)–(4), (8), and (9) should also be coupled with the equations below for calculating the viscoelastic drag experienced by each bubble:

$$\frac{dD_{ve}^{(i)}}{dt} + \left(\frac{1}{\lambda_1} - \frac{\dot{R}_i}{R_i}\right)D_{ve}^{(i)}$$
$$= 12\pi R_i \left[\frac{G}{\lambda_1}(x_i - x_0^{(i)}) + \frac{\mu}{\lambda_1}\dot{x}_i + \frac{\mu\lambda_2}{\lambda_1}\ddot{x}_i\right], \quad i = \{1, 2\}.$$
$$(15)$$

When setting certain viscoelastic parameters to zero (Table I), Eq. (15) can be reduced to the Maxwell, Zener, and Jeffreys viscoelastic drags.

III. RESULTS

In our simulations, the parameters were set according to Table II. Unless specified otherwise, the viscosity μ was set to 0.015 Pa s, the elasticity G was set to 10^5 Pa, the relaxation time λ_1 was set to 3×10^{-9} s, and the retardation time λ_2 was set to 3×10^{-10} s. The equations were solved numerically using the Dormand-Prince fourth-order Runge-Kutta method with the use of an adaptive step size for controlling purposes [62].

A. Verification and validation

In Ref. [34], the currently used single-bubble dynamics model was verified with the analytical and numerical results of other authors. Comparison of the single-bubble dynamics with the experimental data will be performed in the current section for both viscous [70] and viscoelastic media [71]. Since there is no data available for the motion of multiple bubbles in a viscoelastic medium, the validation of the current model for the motion of multiple bubbles will be performed through comparisons with the numerical results of other authors [23] for viscous fluids. Multiple bubble dynamics in a viscoelastic medium will be investigated in the following sections.

In Fig. 2(a), the present results are compared to the experimental data described in Ref. [70]. In Ref. [70], contrast agent bubbles with a lipid monolayer coating on a gas microbubble were considered. The data were measured by a high-speed camera, operated at several millions of frames per second.

TABLE II. Simulation parameters.

Nomenclature	Definition	Value	Source
ρ_t	Density of the biological fluid	$1060\,\text{kg/m}^3$	[63,64]
f	Ultrasound frequency	$10^6\,\text{Hz}$	[4]
A	Ultrasound amplitude	$10^6\,\text{Pa}$	[4]
p_0	Static background pressure	$1.013 \times 10^5\,\text{Pa}$	[32]
S	Surface tension	$0.056\,\text{kg/s}^2$	[32,65]
c_∞	Speed of sound	$1540\,\text{m/s}$	[32,65]
G	Elasticity of the biological fluid	$10\text{–}10^6\,\text{Pa}$	[32,35,66,67]
λ_1	Relaxation time of the biological fluid	$10^{-11}\text{–}10^{-7}\,\text{s}$	[33,35]
μ	Viscosity of the biological fluid	$0.001\text{–}2\,\text{Pa s}$	[68]
n	Constant in GAZ model	7	[45]
B	Constant in GAZ model	$c_\infty^2 \rho_t/n - p_0$	[45]
γ	Specific heat ratio for the bubble's interior	1.4	[69]
λ_2	Retardation time of the biological fluid	$10^{-11}\text{–}10^{-9}\,\text{s}$	[33]

The acoustic pulse was in the form $p(t) = A \cos(2\pi f t)$. It consisted of repeated pulses separated by 60 ms, with increasing amplitudes of $A = 200 \times 10^3$ Pa, 250×10^3 Pa, and 300×10^3 Pa. To perform the comparison, surface tension was considered to be a function of bubble radius (proposed in Ref. [70]).

The verification of the current model and numerical solution for the bubbles' translational motion was performed
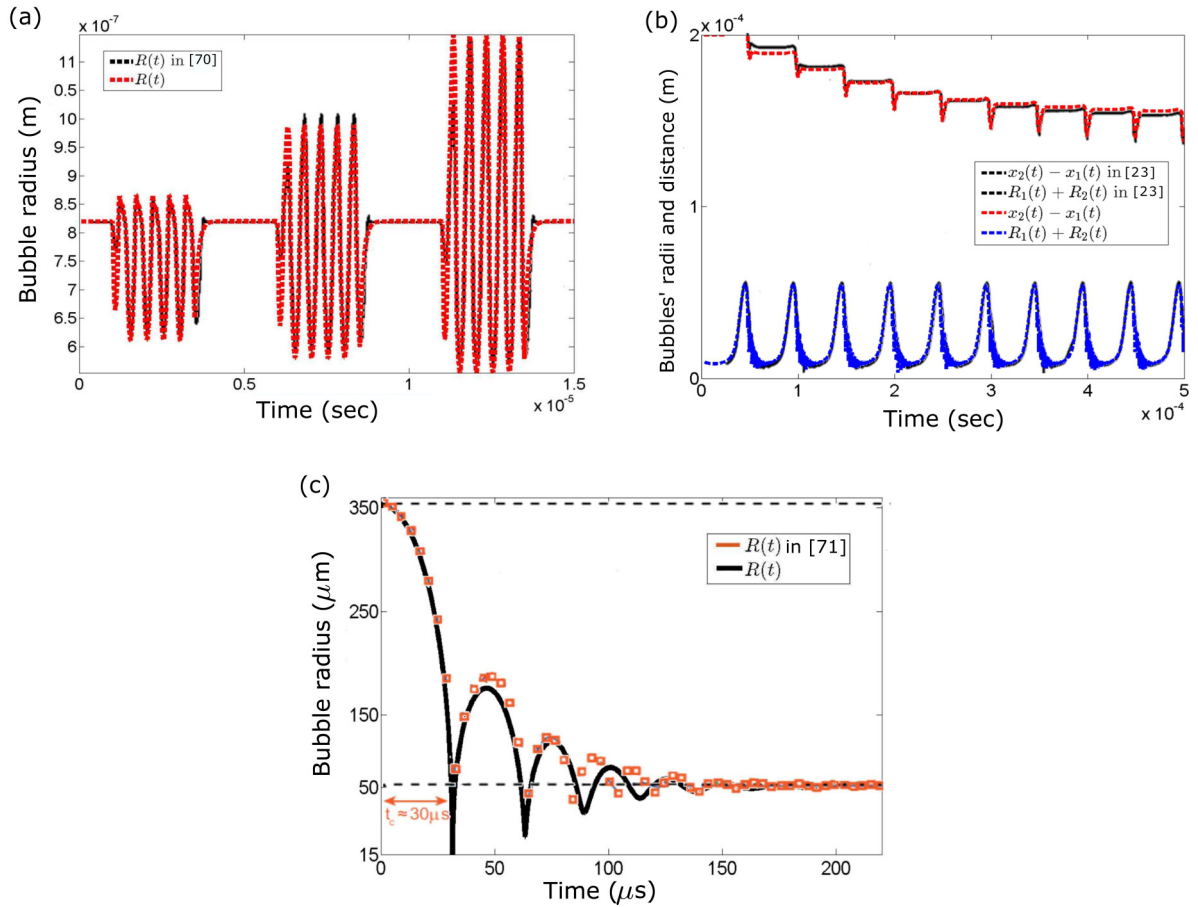

FIG. 2. Validation and verification of the current model by comparing our results with the available experimental and numerical data. $R(t)$ is a bubble radius. (a) Comparison with the experimental data presented in Ref. [70]. $f = 2.9 \times 10^6$ Hz, $R_0 = 0.975\ \mu$m, $c_\infty = 1480$ m/s, $\rho_t = 1000\,\text{kg/m}^3$, $\sigma = \sigma(R)$ [70], $\mu = 0.001$ Pa s, $G = 0$ Pa, $\lambda_1 = 0$ s. (b) Comparison with the simulation results presented in Ref. [23]. $A = 1.21 \times 10^5$ Pa, $f = 20 \times 10^3$ Hz, $R_0^{(1)} = 6\ \mu$m, $R_0^{(2)} = 4\ \mu$m, $x_0^{(1)} = 0\ \mu$m, $x_0^{(2)} = 200\ \mu$m, $c_\infty = 1500$ m/s, $\rho_t = 998\,\text{kg/m}^3$, $\sigma = 0.0725\,\text{kg/s}^2$, $\mu = 0.001$ Pa $\times$ s, $G = 0$ Pa, $\lambda_1 = 0$ s. (c) Comparison with the experimental data presented in Ref. [71]. $p(t) = 0$, $R_0 = 355\ \mu$m ($R_{\text{equilibrium}} = 55\ \mu$m), $c_\infty = 1430$ m/s, $\rho_t = 1060\,\text{kg/m}^3$, $\sigma = 0.056\,\text{kg/s}^2$, $\mu = 0.089$ Pa s, $G = 10^4$ Pa, $\lambda_1 = 0$ s, $\lambda_2 = 0$ s.

through comparison with the case presented in Ref. [23]. It consists of dynamically oscillating the distance between two noncolliding bubbles with the sole viscous forces being considered. As shown in Fig. 2(b), the current results exhibit a very good agreement with those in Ref. [23].

The behavior of a single bubble in the viscoelastic medium was validated with the very recent experimental data presented in Ref. [71]. The results in Ref. [71] showed the inertial collapse of the large bubble generated by the short laser pulse in the polyacrylamide. The pressure inside the bubble was simulated as a function of the bubbles' interior temperature and vapor mass transfer through the bubbles' surface. The Kelvin-Voigt viscoelastic model was used in the validation. As shown in Fig. 2(c), the agreement between the present solution and the experimental observations is quite good. Note that later in the current research, the simplified equations for the bubbles' interior will be used (Sec. II A).

To the best of the authors' knowledge, an experimental study on multiple bubble dynamics in a viscoelastic medium has not yet been performed. Hopefully, the present study will motivate some experimental groups to investigate this topic.

B. Effect of the presence of nearby bubbles on the single-bubble dynamics

In the majority of studies, single-bubble dynamics are investigated. However, in real biomedical applications, bubble clouds are quite often present. In the current subsection, the effect of bubble-bubble interactions on the dynamics of a single bubble is examined. For these purposes, bubble dynamics obtained from the isolated bubble model is compared to the one calculated using the bubble-bubble interaction model with different viscoelastic drags.

As shown in Fig. 3, single-bubble oscillations are noticeably affected by the presence of nearby bubbles compared to the case of an isolated single bubble. This behavior can be observed in the case where bubbles are placed relatively close to each other (initial distance was $x_0^{(2)} - x_0^{(1)} = 170 \ \mu$m). However, in the limiting case, when the distance between the bubbles is large enough (Fig. 4), the single-bubble dynamics solutions of the bubble-bubble interaction model and the isolated bubble model coincide. Two drags were studied in Fig. 3, namely, viscous Levich drag [Eq. (10)] and viscoelastic drag in the Zener form [Eq. (15)]. It was shown that radial oscillations of the bubble are not affected by the choice of the viscoelastic drag. Being an external force, viscoelastic drag is expected to affect the translational motion of the bubbles rather than their radial motion.

As shown in Fig. 4, with increasing initial distance d_0 between the bubbles, the effect of the second bubble on the first bubble is negligible. To determine the distance at which the impact of the surrounding bubbles on the radial motion of the single bubble can be neglected, the new variable ζ is introduced. The variable ζ is chosen in a form of the relative error measured between the solution curves in the case of the bubbles being isolated from each other and the case of the bubble-bubble interaction being taken into account. The
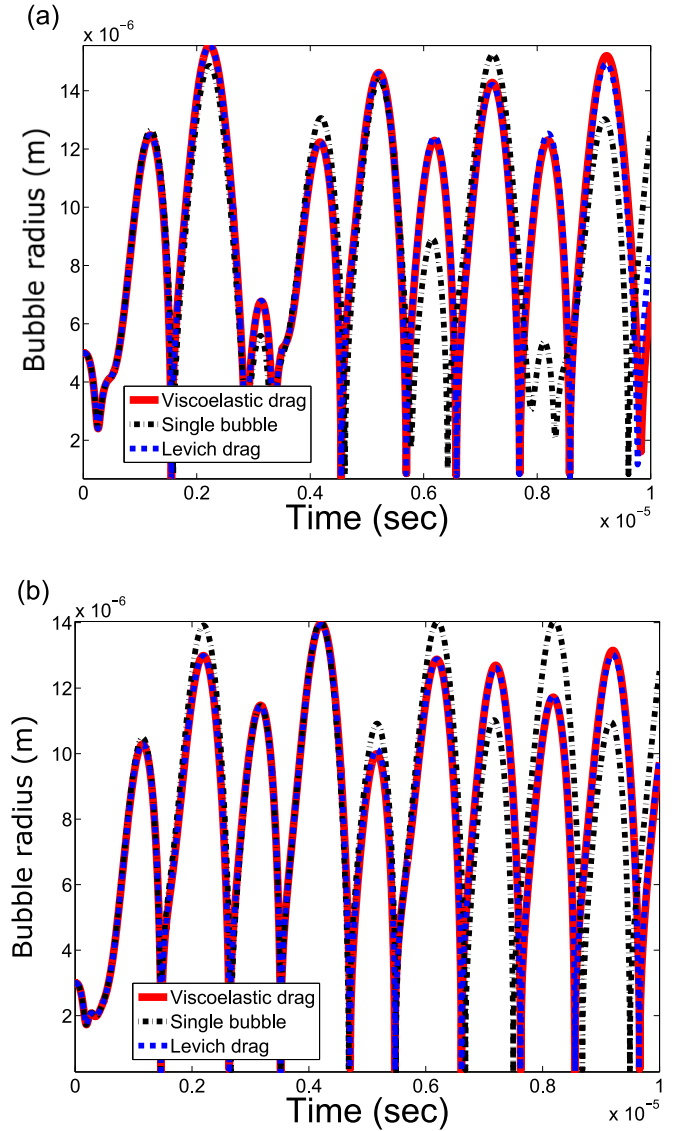

(a)

(b)

FIG. 3. The effect of the presence of the surrounding bubbles and viscoelastic nature of the drag on the single-bubble dynamics. Three cases were considered (on the basis of the Gilmore-Akulichev-Zener model): single isolated bubble, bubble-bubble interaction model with Levich viscous drag, and bubble-bubble interaction model with viscoelastic drag in a Zener form. (a) The first bubble dynamics. (b) The second bubble dynamics. $R_0^{(1)} = 5 \ \mu$m, $R_0^{(2)} = 3 \ \mu$m, $x_0^{(1)} = 0 \ \mu$m, $x_0^{(2)} = 170 \ \mu$m. $\mu = 0.015$ Pa s, $G = 10^5$ Pa, $\lambda = 3 \times 10^{-9}$ s.

variable ζ is defined as follows:

$$\zeta = \left\| \frac{R_1^{\text{isolated}}(t) + R_2^{\text{isolated}}(t)}{R_1(t) + R_2(t)} - 1 \right\|_{L^2}, \tag{16}$$

where $R_1^{\text{isolated}}(t)$ and $R_2^{\text{isolated}}(t)$ are the radii of the first and second bubbles being isolated from each other. The norm cast in L^2 is defined as follows: $\|g(t)\|_{L^2} = [\frac{1}{T} \int_0^T g(t)^2 dt]^{\frac{1}{2}}$, where T is several periods of the driving pressure (currently, T was set to 10 periods). In the present research, $\zeta = 0.1$ is chosen to be a threshold value such that if ζ is smaller than the chosen threshold, the effect is considered to be negligible (Fig. 4). Note that the threshold value $\zeta = 0.1$ can be slightly corrected
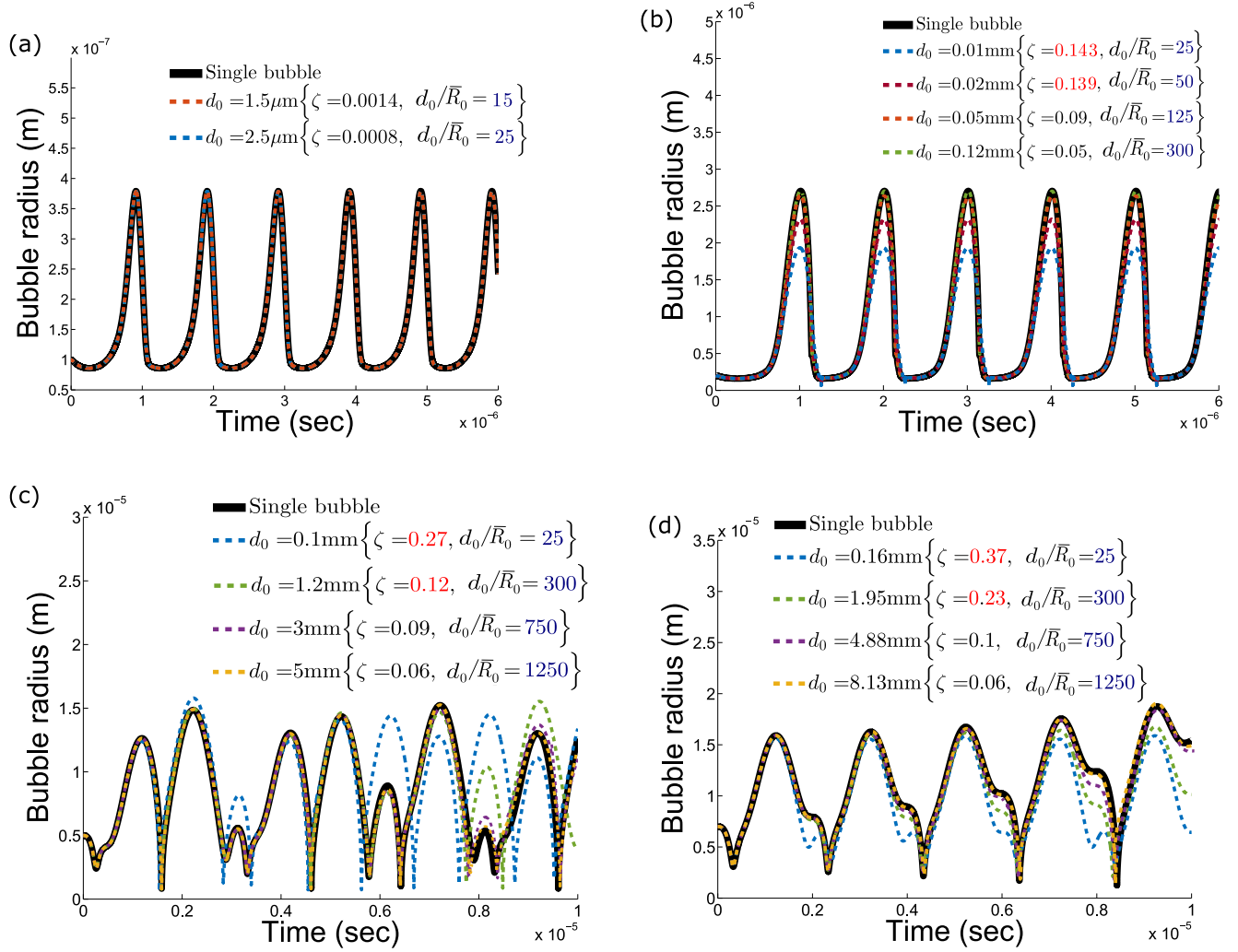
FIG. 4. The effect of the presence of the surrounding bubbles on the single-bubble dynamics for different initial distances d_0 between the bubbles. The solid black line denotes the dynamics of the isolated bubble. When $\zeta \leqslant 0.1$, the effect can be neglected. When $\zeta > 0.1$, the effect is noticeable (red font). $\overline{R}_0 = [R_0^{(1)} + R_0^{(2)}]/2$. (a) $R_0^{(1)} = 0.1\ \mu$m, $R_0^{(2)} = 0.1\ \mu$m. (b) $R_0^{(1)} = 0.6\ \mu$m, $R_0^{(2)} = 0.2\ \mu$m. (c) $R_0^{(1)} = 5\ \mu$m, $R_0^{(2)} = 3\ \mu$m. (d) $R_0^{(1)} = 7\ \mu$m, $R_0^{(2)} = 6\ \mu$m. The viscoelastic parameters are $\mu = 0.015$ Pa s, $G = 10^5$ Pa, $\lambda = 3 \times 10^{-9}$ s.

according to the desired accuracy of simulations. However, the authors consider the present threshold value $\zeta = 0.1$ to be already a good choice in terms of the calculations' accuracy.

In Fig. 4, the effect of bubble-bubble interactions on the dynamics of a single bubble is shown for several different bubble radii and distances between bubbles. The initial radii of the bubbles ($R_0^{(1)}$ and $R_0^{(2)}$) were varied in the range from 1 to 10 μm. It was determined that at a distance of several millimeters, the effect of bubble-bubble interactions on the dynamics of a single bubble can be neglected (as $d_0/\{[R_0^{(1)} + R_0^{(2)}]/2\} \geqslant$ 750 in Figs. 4(c) and 4(d) for micron-sized bubbles). For very small bubbles (on the order of $0.1\ \mu$m and smaller), the effect of the nearby bubbles can be neglected even at short distances [$\zeta < 0.1$ at $d_0/\{[R_0^{(1)} + R_0^{(2)}]/2\} \leqslant 15$ in Fig. 4(a)]. This phenomenon occurs only for small bubbles due to the correspondingly small amplitude of bubble oscillations that can be observed in Fig. 4(a).

Note that the effect of other bubbles on the current bubble's radial motion is dependent on the viscoelastic properties of the biological fluid in which these bubbles are located.

Therefore, later in this section, the effect of nearby bubbles will be studied with respect to the viscoelastic features of the medium.

The elasticity of the surrounding medium is known to dampen bubble radial oscillations (as was shown in the previous studies [33–36,72]). This pattern can still be observed in the current model [Fig. 5(a)]. Since the amplitude of bubbles' oscillations is much smaller at high elasticities, their influence on each other should also be less, even at quite short distances between them. This can indeed be observed in Figs. 6(a) and 6(c), where for highly elastic fluids, the effect of the nearby bubble can be neglected even at small initial distances between the bubbles ($d_0 = 50\ \mu$m). Thus, at high elasticity values, even the bubbles that are located close to each other will not significantly affect each other's radial motion.

Bubbles' oscillations are well known to be reduced by the viscosity of the medium [34]. Therefore, with increasing viscosity, the bubbles' influence on each other also decreases [Figs. 6(a) and 6(b)]. In highly viscous fluids, the impact of other bubbles on the current bubble can be neglected even
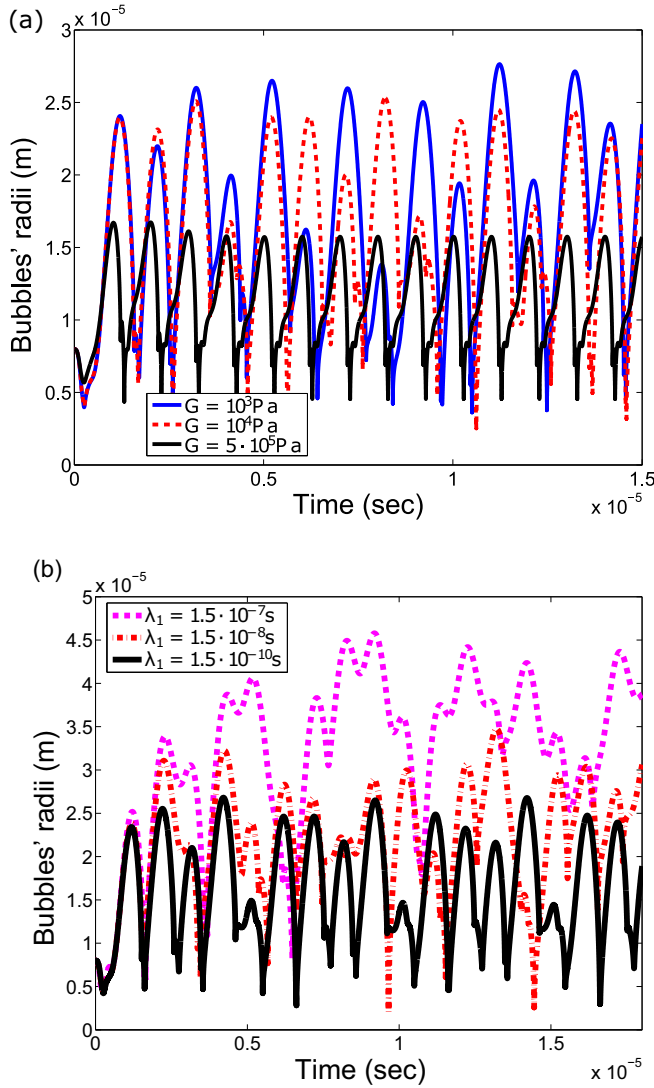
FIG. 5. Viscoelastic effects on the bubbles' radial motion. (a) Elasticity effect. Sum of bubble radii $R_1(t) + R_2(t)$ plotted for the case of $x_0^{(1)} = 0$ m, $x_0^{(2)} = 200$ μm, $\lambda_1 = 3 \cdot 10^{-10}$ s. (b) Relaxation time effect. Sum of bubble radii $R_1(t) + R_2(t)$ plotted for the case of $x_0^{(1)} = 0$ m, $x_0^{(2)} = 200$ μm, $G = 3 \cdot 10^3$ Pa. $R_0^{(1)} = 5$ μm, $R_0^{(2)} = 3$ μm. $\mu = 0.015$ Pa s.

for the case where bubbles are placed at short distances ($d_0 = 50$ μm in Fig. 6).

The relaxation time is the time that is required for the viscoelastic material to return back to the unperturbed state. Thus, it is expected that small relaxation times of the medium will suppress the radial motions of the bubbles since the material permits a fast return to the undisturbed state. The relaxation time effect is shown in Fig. 5(b). Due to the use of the new viscoelastic coupling equations Eqs. (8) and (9), an increase in the relaxation time results in less damping on the bubble oscillations and faster growth of the bubble (Fig. 5(b), which is in accordance with [33]). Since bubbles' oscillations are larger at longer relaxation times, their influence on each other is also larger. In Figs. 6(b) and 6(c), it is shown that an increase in the relaxation time of the medium also enlarges the initial distance at which bubbles do not impact each
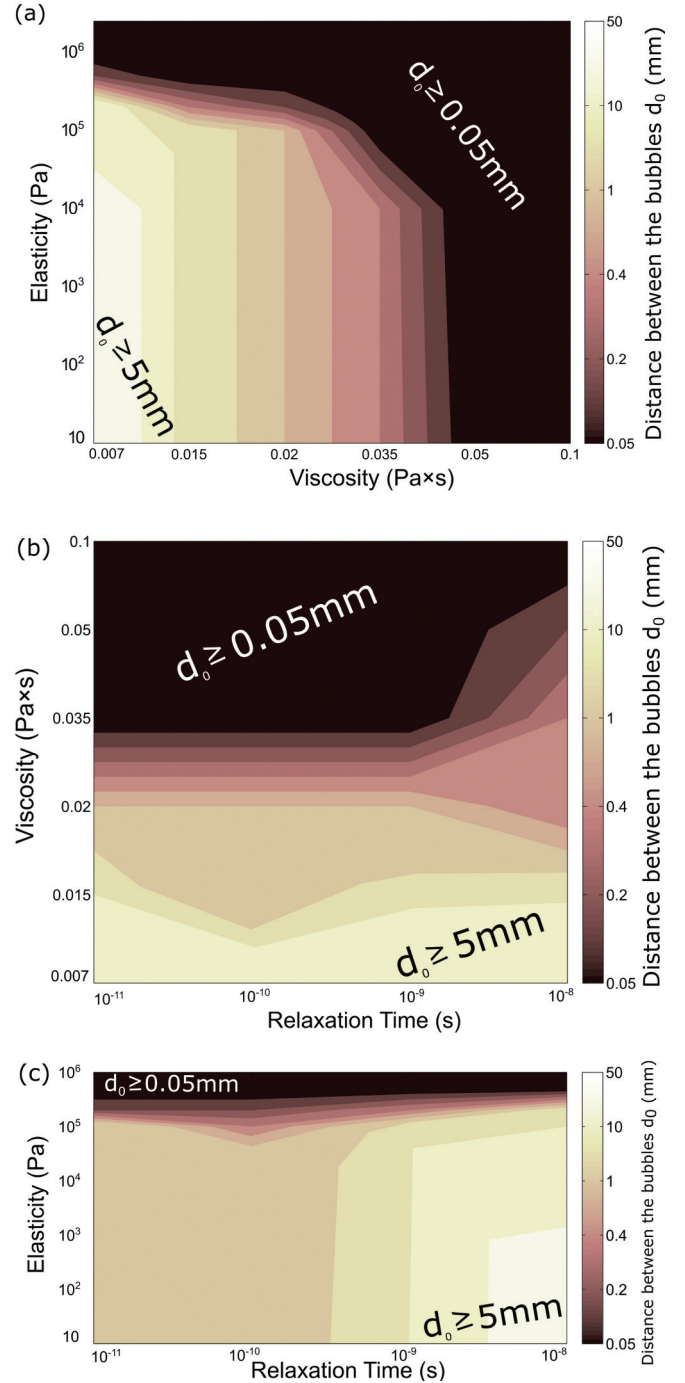

FIG. 6. The distance d_0 between bubbles at which their effect on each other is negligible ($\zeta \leqslant 0.1$), plotted for different viscoelastic properties of the medium. (a) Variation of the elasticity and viscosity of the medium, $\lambda_1 = 3 \times 10^{-9}$ s. (b) Variation of the relaxation time and viscosity of the medium, $G = 10^5$ Pa. (c) Variation of the elasticity and relaxation time of the medium, $\mu = 0.015$ Pa s. $R_0^{(1)} = 5$ μm, $R_0^{(2)} = 3$ μm.

other's radial motion. However, the relaxation time effect is not dominant; it can be observed only at moderate values of elasticity and viscosity.

It can be concluded that the presence of nearby bubbles noticeably affects the dynamics of a single bubble. The consideration of multiple bubbles makes the radial motion of a
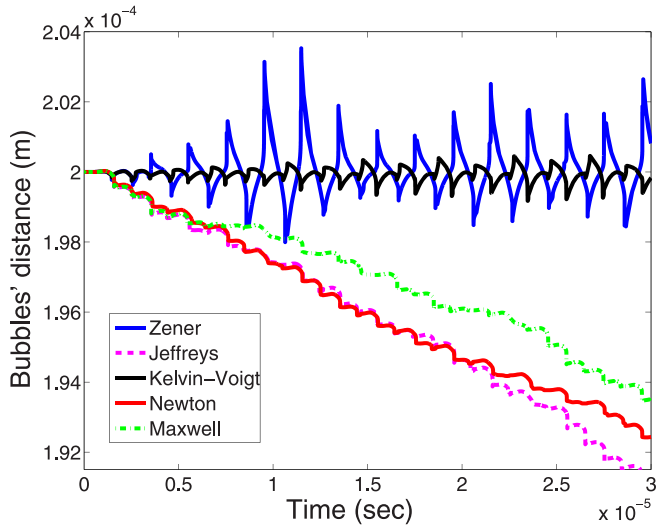
FIG. 7. Distance between the bubbles for the Zener, Maxwell, Newton, and Kelvin-Voigt viscoelastic models with the corresponding viscoelastic drags. $R_0^{(1)} = 5$ μm, $R_0^{(2)} = 3$ μm, $x_0^{(1)} = 0$ μm, $x_0^{(2)} = 200$ μm.

single bubble more complicated. However, depending on the viscoelastic properties of the medium in which the bubbles are located, the effect of other bubbles' presence can occasionally become negligibly small. This effect becomes negligible with increasing elasticity and viscosity of the biological fluid, as well as with decreasing relaxation time.

C. Comparison of different viscoelastic drags

Although the viscoelastic properties of the drag do not impact single-bubble dynamics (Sec. III B), they are expected to significantly change the translational motion of the bubbles. As is known, various viscoelastic models exist. In the current subsection, the translational motion of the bubbles is examined with respect to different types of viscoelastic media, i.e., different viscoelastic drags.

With the current parameters (Table II), bubbles in a Newtonian fluid are observed to be drawn to each other with time (Fig. 7). In addition to the attraction of the bubbles, the dynamical steady state of the distance between the bubbles can be observed in the present case. Dynamical steady state means that the distance between bubbles does not remain constant; however, its oscillations are sufficiently small, and the average value over several periods is constant. This stably oscillating distance between the bubbles can be observed only for models that account for the elasticity of the surrounding medium (i.e., Zener and Kelvin-Voigt models). In contrast, for the Maxwell, Jeffreys, and Newton models, bubbles are drawn to each other.

With a long calculation time, it is even more obvious that the elastic properties of the drag force play the key role in the bubbles' translational motion. The dynamical steady state of the distance between the bubbles is obtained for Zener viscoelastic drag [Fig. 8(a)]. When considering Levich viscous drag, bubbles tend to collide [Fig. 8(b)].

It can be concluded that the elastic properties of the drag in the viscoelastic surrounding medium cannot be ignored
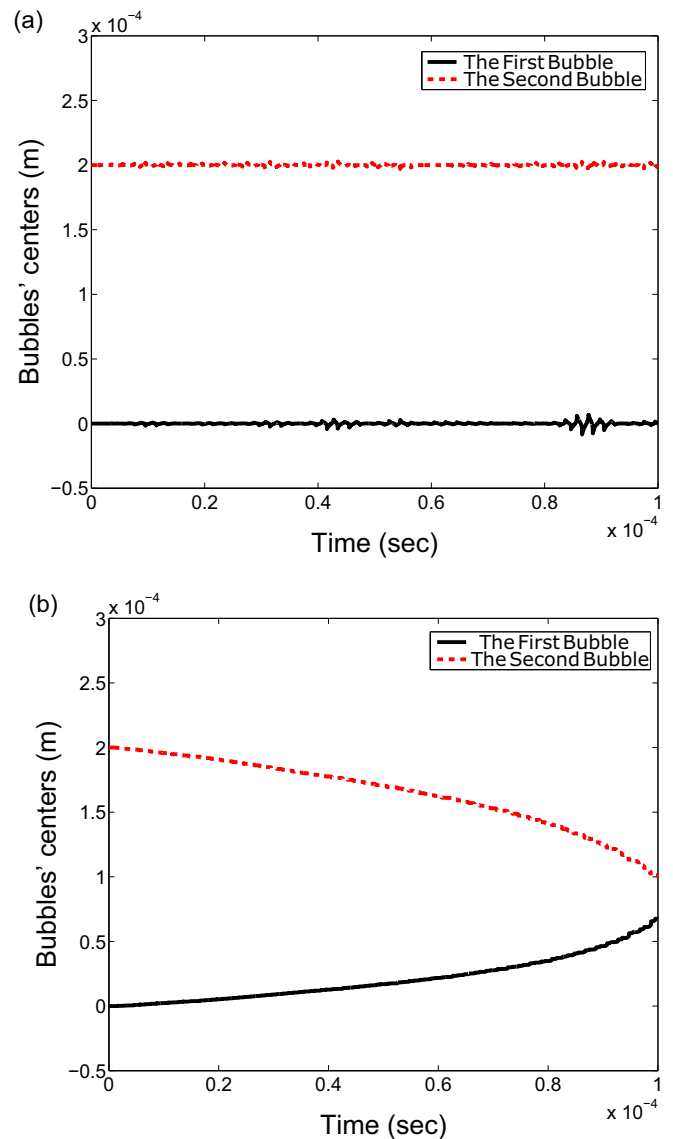

FIG. 8. Viscoelastic drag effect. (a) Motion of the bubble centers exerted by Zener viscoelastic drag. (b) Motion of the bubble centers exerted by Levich viscous drag. $R_0^{(1)} = 5$ μm, $R_0^{(2)} = 3$ μm, $x_0^{(1)} = 0$ μm, $x_0^{(2)} = 200$ μm.

because they noticeably resist the translational motion of the bubbles and prevent their collision. A further discussion of the influence of the viscoelastic properties of the medium on the bubbles' translational motion, as well as their variation, is presented in Sec. III D.

In Figs. 7 and 8, in the case of the absence of the elasticity component in the drag, the attraction of bubbles can be observed. However, in general, this attraction is not the only possible pattern of the bubbles' motion. It is known that pulsating bodies in fluid either attract each other, when they oscillate in phase, or repel each other, when they oscillate in antiphase (as was discovered by Bjerknes and Bjerknes [73,74]). In particular, according to the classical theory of the secondary Bjerknes force, there are two scenarios of bubbles' behavior. If the frequency of the driving pulse is between the bubbles' resonance frequencies (which can be calculated according to

Minnaert's formula [75,76]), then bubbles are repelled. In all other cases, bubbles are attracted to each other. However, recent experimental and theoretical studies [23,30,76–83] have shown that bubbles do not always behave in agreement with the classical Bjerknes theory, and their dynamics are more complicated. Several new effects have been observed. With increasing amplitude of the driving pulse, the direction of the secondary Bjerknes force can be different from that in the classical Bjerknes theory [79]. With decreasing distance between the bubbles, for the bubbles driven below resonance, the secondary Bjerknes force can change sign, leading to the formation of the effect known as "bubble grapes" (stable clusters of large bubbles with persistent separation distances comparable to the bubbles' sizes [80,81,84]). Bubbles can be in the regime of stable periodic translational motion that is not present in the classical Bjerknes theory [23,82,83]. In this case, the dynamical equilibrium distance exists, which can be an explanation of the effect known as "acoustic streamers," when in a strong acoustic field, bubbles group themselves in branched filamentary structures [23,76]. The mechanisms causing the new regimes of the bubbles' motion are not very clear, and they are currently still under investigation. One of the profound studies on bubbles' motion can be found in Ref. [77], in which the refined Bjerknes theory is proposed, which includes some newly observed regimes of the bubbles' motion. The equations derived in Ref. [77] (that correspond to the bubble-bubble interaction model) are similar to the currently used ones [23,25].

With the current simulation parameters, bubbles being repelled from each other are difficult to observe. First, in the current one-dimensional model, the space propagation of the ultrasound wave has not been taken into account. However, consideration of the space propagation of the wave (which should be taken into account in the three-dimensional model, as mention ed in Sec. II A) can lead to bubbles' oscillations being in antiphase and thus their repulsion. Second, a high frequency (and amplitude) of the driving pulse has been considered. However, by using the lower ultrasound frequency (and amplitude), slight repulsion of bubbles can be captured on the basis of the current model with consideration of Levich drag (Fig. 9). Nevertheless, the regimes of the bubbles' motion are not the objective of the current investigation. The present study is focused on illustrating how the newly derived viscoelastic drag affects bubbles' motion (where the motion itself can be either attractive, repulsive, or shifting between those two). In Fig. 9, it can be observed that the effect of the viscoelastic drag in the case of the bubbles' repulsion is analogous to that in the case of the bubbles' attraction (Fig. 8). Later in this paper, ultrasound of high frequency and amplitude will be considered, while the consideration of lower frequencies and amplitudes of the driving pulse can be investigated in future studies.

Note that at lower ultrasound intensities, the inclusion of viscoelastic features of the medium might switch the direction of the bubbles' interaction force. This might occur due to the change in the frequencies of the bubbles' oscillations associated with the viscoelastic effects on bubble dynamics (discussed in Sec. II A). Nevertheless, at the currently considered case of high ultrasound frequency and amplitude, this behavior has not been observed.
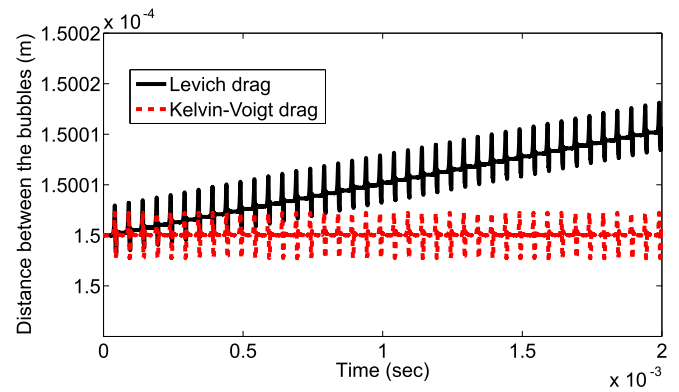

FIG. 9. Repulsion of the bubbles at lower ultrasound frequencies (and amplitudes, $A = 1.3 \times 10^5$ Pa, $f = 20 \times 10^3$ Hz). The black line is the distance between bubble centers experiencing the Levich viscous drag. The red line is the distance between bubble centers experiencing the Kelvin-Voigt viscoelastic drag. $R_0^{(1)} = 3\ \mu$m, $R_0^{(2)} = 2\ \mu$m, $x_0^{(1)} = 0\ \mu$m, $x_0^{(2)} = 150\ \mu$m, $G = 2 \times 10^3$ Pa.

D. Influence of the viscoelastic properties of the medium on the bubbles' translational motion

The viscoelastic parameters can vary in a wide range for different biological materials. For example, the elasticity can range from 0 to 10 MPa [32,35,66,67]. Thus, it is important to understand how viscoelastic features of the medium can impact the dynamics of multiple bubbles. In Sec. III C, it was shown that viscoelastic parameters such as elasticity and relaxation can affect the bubbles' translational motion. The easiest model that takes both elasticity and relaxation time into account is the Zener model. Moreover, by varying the viscoelastic parameters, the Zener model can be reduced to all other considered viscoelastic models, except the Jeffreys model. Therefore, for studying elasticity, viscosity, and relaxation time effects, the description of the surrounding medium was chosen to be in the Zener form, while the retardation time effect was examined based on the Jeffreys model.

The effect of the viscoelastic features on the bubbles' translational motion is summarized in Fig. 10. Because viscosity is known to resist the movement of bubbles in space, the elasticity and relaxation time effects were studied with respect to different viscosity values. In Fig. 10, it can be observed that in fluids with either high elasticity or viscosity (or both), bubbles will remain near their initial locations in space. Thus, as stated in Sec. III C, increasing elasticity tends to resist translational motion of the bubbles (as also shown in Fig. 11). At low values of elasticity and viscosity, at the currently used parameters, bubbles are attracted toward each other (Fig. 10).

Two patterns of the relaxation time effect were revealed (Fig. 12). Figure 12(a) shows that larger relaxation times cause larger oscillations of the bubbles' spacing. However, the effect will vanish at high viscosity values (Fig. 10). Meanwhile, with decreasing elasticity of the medium $G \to 0$, larger relaxation times of the medium start to accelerate bubbles' attraction (Fig. 12(b): $\lambda > 10^{-9}$ s, Fig. 10).

The retardation time λ_2 effect was studied on the basis of the Jeffreys model. However, its contribution was found to be not significant.
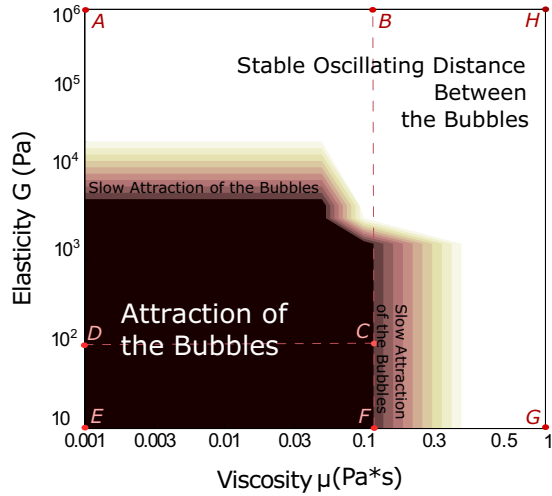
FIG. 10. Viscoelastic effects on the translational bubbles' motion at high ultrasound frequency and amplitude. Zones of the relaxation time effect are shown by Latin letters. The area $ABCD$: relaxation time enlarges the oscillations of the bubbles' distance. The area $CDEF$: large relaxation times accelerate bubbles' attraction. The area $FGHB$: relaxation time effect vanishes.

Overall, there is a significant difference between the motion of bubbles in the viscoelastic medium in comparison with the viscous medium. The elasticity of the biological fluid is the key parameter that affects the translation motion of bubbles. Moreover, the relaxation time effect was also found to be very important.

IV. CONCLUSIONS

Due to the rapid emergence of biomedical applications, interest in the motion of bubbles in viscoelastic media has recently increased. Most of the previous studies regarding the motion of multiple bubbles have been performed in
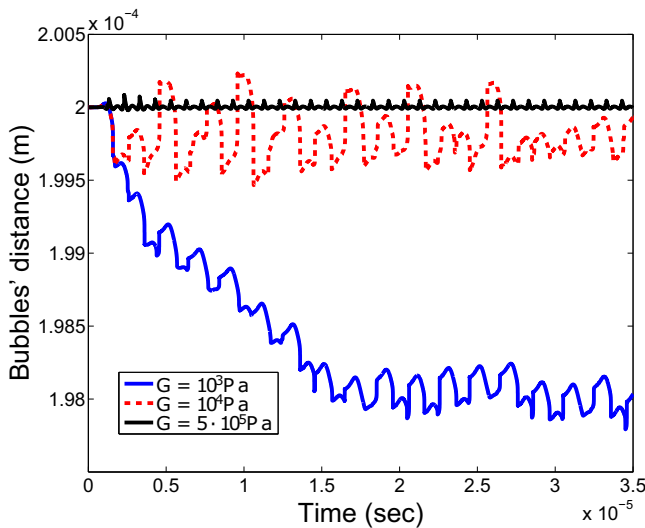

FIG. 11. Elasticity effect on the distance between the bubbles $d(t) = x_2(t) - x_1(t)$. $R_0^{(1)} = 5$ μm, $R_0^{(2)} = 3$ μm, $x_0^{(1)} = 0$ m, $x_0^{(2)} = 200$ μm, $\lambda_1 = 3 \cdot 10^{-10}$ s, $\mu = 0.015$ Pa s.
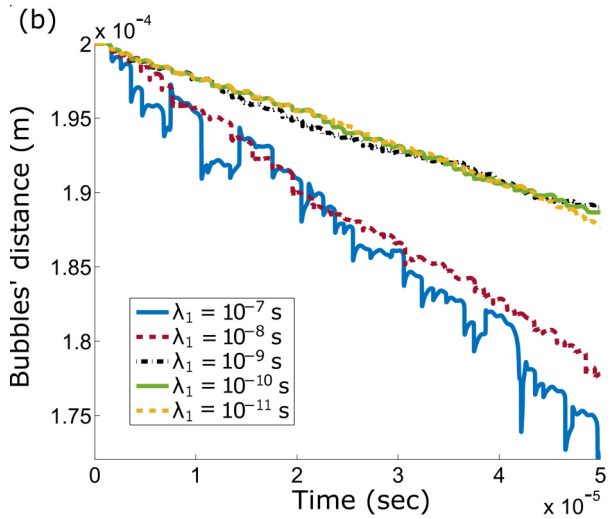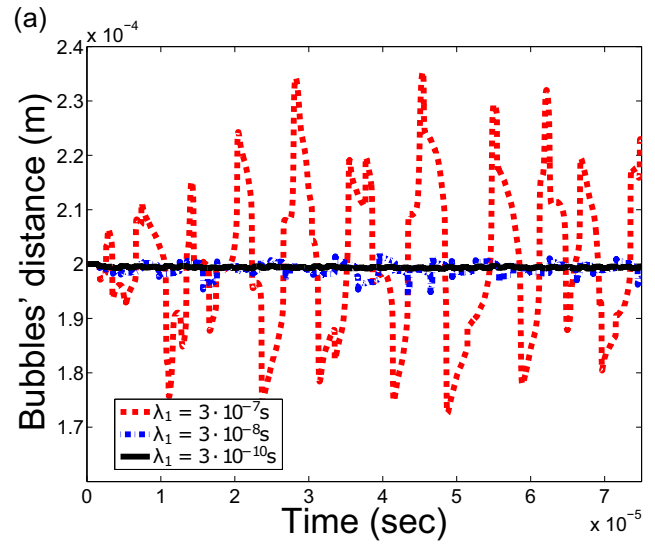

FIG. 12. Relaxation time effect on the distance between the bubbles $d(t) = x_2(t) - x_1(t)$. (a) $G = 10^4$ Pa. (b) $G = 10$ Pa. $R_0^{(1)} = 5$ μm, $R_0^{(2)} = 3$ μm, $x_0^{(1)} = 0$ m, $x_0^{(2)} = 200$ μm, $\mu = 0.015$ Pa s.

Newtonian fluids. In the present paper, a study of bubble-bubble interactions in viscoelastic media was performed. To achieve the above goal, the bubble-bubble interaction model in the Newtonian fluid [23] was generalized for viscoelastic media. To elucidate the viscoelastic features of the medium surrounding the bubbles that impact bubbles' translational motion, the relation for viscoelastic drag was derived.

For different applications and materials, different viscoelastic models can be suitable. Therefore, the viscoelastic drag equations were derived for different viscoelastic models. The elasticity of the surrounding medium was revealed to be the key parameter in terms of the bubbles' translational motion (in addition to the viscosity being conventionally taken into account). It was shown that the elastic features of the surrounding medium significantly resist translational motion of the bubbles. For the parameters considered in the current paper, the bubbles are drawn to each other in the Newtonian fluid. Conversely, if the elasticity of the medium is taken into

account, a dynamical steady state for the distance between the bubbles can be achieved.

In modern biomedical applications, the ultrasound driving pulse can be of high amplitude. Therefore, the Gilmore-Akulichev cavitation model was chosen to simulate the bubble's radial motion. To allow the radial motion of a single bubble to be affected by the viscoelasticity of the surrounding medium, the cavitation model was also coupled with the viscoelastic model. Thus, in the model proposed in the current research, both the translational and radial motions of the bubbles are affected by the viscoelastic features of the medium.

Most of the theoretical studies are focused on the dynamics of a single bubble. However, in the majority of biomedical applications, bubble clouds are present. Thus, the study on the radial motion of a single bubble in the multiple-bubble model was performed. It was concluded that single-bubble dynamics are noticeably affected by the presence of the nearby bubbles. However, with increasing distance between the bubbles up to several millimeters, their influence on each other vanishes. The influence of bubbles on each other strongly depends on the viscoelastic properties of the medium in which the bubbles are located. Increasing elasticity and viscosity, as well as decreasing relaxation time, of the medium decreases the effect of other bubbles on the radial motion of the current bubble (thereby shortening the distance at which this effect is negligible).

A parametric study with respect to the viscoelastic properties of the medium was conducted. The effect of the viscoelasticity on the radial behavior of a single bubble has already been studied by different authors. The current study investigated its effect on the translational motion of multiple bubbles. The elasticity of the biological fluid (as well as conventionally taken into account viscosity) significantly resists the translational motion of the bubbles. At high and moderate elasticity values, the relaxation time of the surrounding medium can cause larger oscillations of the distance between the bubbles, whereas at small elasticity values, large relaxation times start to accelerate the movement of bubbles in space. It can be concluded that both elasticity G and relaxation time λ_1 are

very important. After the evaluation of the viscoelastic models considered in the current paper, the Zener model was found to be the most appropriate one since it accounts for both the elasticity and the relaxation time.

The present model, based on the relatively simple model described in Ref. [23], attempts to clarify the impact of the newly derived viscoelastic drag on the dynamics of bubble-bubble interactions. In the future, the current model is going to be expanded to take the three-dimensional movement of multiple bubbles into account (based on Ref. [24]).

APPENDIX A: COUPLING STRESS EQUATION FOR VISCOELASTIC MODELS OF MAXWELL FAMILY

To make the derivation more intuitive, the variables in strain are separated:

$$\gamma_{rr} = X(r)Y[R(t)] = X(r)Y(t),$$

$$X(r) = -\frac{2}{3r^3}, \quad Y(t) = R(t)^3 - R_0^3. \quad \text{(A1)}$$

Using hypotheses of casual histories, the stress-strain integral relationship for viscoelastic fluids is written as follows [85,86]):

$$\tau_{rr} = 2\gamma_{rr}(r,t)|_{t=0+}E(t) + 2\int_0^t E(t-t_1)\frac{d\gamma_{rr}(r,t_1)}{dt_1}dt_1$$

$$= 2X(r)\int_0^t E(t-t_1)\frac{dY(t_1)}{dt_1}dt_1, \quad \text{(A2)}$$

where $E(t - t_1)$ is a relaxation modulus function.

For the viscoelastic models, when $\lambda_1 \neq 0$, the relaxation modulus function can be written as $E(t) = G + \frac{\mu\lambda_2}{\lambda_1}\delta(t) + (\frac{\mu}{\lambda_1} - \frac{\mu\lambda_2}{\lambda_1^2} - G)e^{-\frac{t}{\lambda_1}}$ (Table I, [85]). Then, one can obtain

$$\tau_{rr} = 2X(r)\int_0^t \left[G + \frac{\mu\lambda_2}{\lambda_1}\delta(t-t_1) + \left(\frac{\mu}{\lambda_1} - \frac{\mu\lambda_2}{\lambda_1^2} - G\right)e^{\frac{t_1-t}{\lambda_1}} \right]\frac{dY(t_1)}{dt_1}dt_1$$

$$= 2X(r)GY(t) + 2X(r)\frac{\mu\lambda_2}{\lambda_1}\frac{dY(t)}{dt}[2\theta(t) - 1] + 2X(r)\left[\frac{\mu}{\lambda_1} - \frac{\mu\lambda_2}{\lambda_1^2} - G\right]\int_0^t e^{\frac{t_1-t}{\lambda}}\frac{dY(t_1)}{dt_1}dt_1. \quad \text{(A3)}$$

In the above equations, $\theta(t)$ is a Heaviside function.
At $r = R$, Eq. (A3) is written as

$$\tau_{rr}|_{r=R} = 2X(R)GY(t) + 2X(R)\frac{\mu\lambda_2}{\lambda_1}\frac{dY(t)}{dt}[2\theta(t) - 1] + 2X(R)\left[\frac{\mu}{\lambda_1} - \frac{\mu\lambda_2}{\lambda_1^2} - G\right]\int_0^t e^{\frac{t_1-t}{\lambda}}\frac{dY(t_1)}{dt_1}dt_1. \quad \text{(A4)}$$

At $t = 0$, $\tau_{rr}|_{r=R}(t = 0) = 0$. The derivative of the stress Eq. (A4) with respect to t (for $t > 0$) is given as follows:

$$
\frac{d\tau_{rr}|_{r=R}}{dt} = 2G\frac{\partial X(R)}{\partial R}\dot{R}Y(t) + 2GX(R)Y_t' + 2\frac{\partial X(R)}{\partial R}\dot{R}\frac{\mu\lambda_2}{\lambda_1}Y_t' + 2X(R)\frac{\mu\lambda_2}{\lambda_1}Y_{tt}''
$$

$$
+ 2\frac{\partial X(R)}{\partial R}\dot{R}\left(\frac{\mu}{\lambda_1} - \frac{\mu\lambda_2}{\lambda_1^2} - G\right)\int_0^t e^{\frac{t_1-t}{\lambda_1}}\frac{dY(t_1)}{dt_1}dt_1 + 2X(R)\left(\frac{\mu}{\lambda_1} - \frac{\mu\lambda_2}{\lambda_1^2} - G\right)Y_t'
$$

$$
- 2X(R)\left(\frac{\mu}{\lambda_1} - \frac{\mu\lambda_2}{\lambda_1^2} - G\right)\frac{1}{\lambda_1}\int_0^t e^{\frac{t_1-t}{\lambda_1}}\frac{dY(t_1)}{dt_1}dt_1
$$

$$
= 2G\frac{\partial X(R)}{\partial R}\dot{R}Y(t) + 2\left(\frac{\mu}{\lambda_1} - \frac{\mu\lambda_2}{\lambda_1^2}\right)X(R)Y_t' + 2\frac{\partial X(R)}{\partial R}\dot{R}\frac{\mu\lambda_2}{\lambda_1}Y_t' + 2X(R)\frac{\mu\lambda_2}{\lambda_1}Y_{tt}''
$$

$$
+ \left(\frac{\partial X(R)}{\partial R}\dot{R}\frac{1}{X(R)} - \frac{1}{\lambda_1}\right)\left[\tau_{rr}|_{r=R} - 2X(R)GY(t) - 2X(R)\frac{\mu\lambda_2}{\lambda_1}Y_t'\right]. \tag{A5}
$$

Equation (A5) can be further written as

$$
\frac{d\tau_{rr}|_{r=R}}{dt} = 2G\dot{R}\frac{\partial X(R)}{\partial R}Y(t) + 2\left(\frac{\mu}{\lambda_1} - \frac{\mu\lambda_2}{\lambda_1^2}\right)\frac{d\gamma_{rr}}{dt}\bigg|_{r=R} + 2\frac{\partial X(R)}{\partial R}\dot{R}\frac{\mu\lambda_2}{\lambda_1}Y_t' + 2\frac{\mu\lambda_2}{\lambda_1}\frac{d^2\gamma_{rr}}{dt^2}\bigg|_{r=R}
$$

$$
+ \left(\frac{\partial X(R)}{\partial R}\frac{1}{X(R)}\dot{R} - \frac{1}{\lambda_1}\right)\left[\tau_{rr}|_{r=R} - 2G\gamma_{rr}|_{r=R} - 2\frac{\mu\lambda_2}{\lambda_1}\frac{d\gamma_{rr}}{dt}\bigg|_{r=R}\right]. \tag{A6}
$$

Then, the above equation can be reduced to

$$
\tau_{rr}|_{r=R}\left(1 + 3\lambda_1\frac{\dot{R}}{R}\right) + \lambda_1\frac{d\tau_{rr}|_{r=R}}{dt} = 2G\gamma_{rr}|_{r=R} + 2\mu\frac{d\gamma_{rr}}{dt}\bigg|_{r=R} + 2\mu\lambda_2\frac{d^2\gamma_{rr}}{dt^2}\bigg|_{r=R}. \tag{A7}
$$

APPENDIX B: DERIVATION OF THE UNSTEADY DRAG ON BUBBLES OF VARIABLE RADII IN THE VISCOELASTIC FLUID

In Ref. [56], by invoking a cell model, the expression of the drag F_D experienced by a bubble of nonconstant volume in viscous fluid was derived. The model is schematically shown in Fig. 13. The cell model simulated a spherical bubble that is restricted by surface S_1. A bubble was changing its size
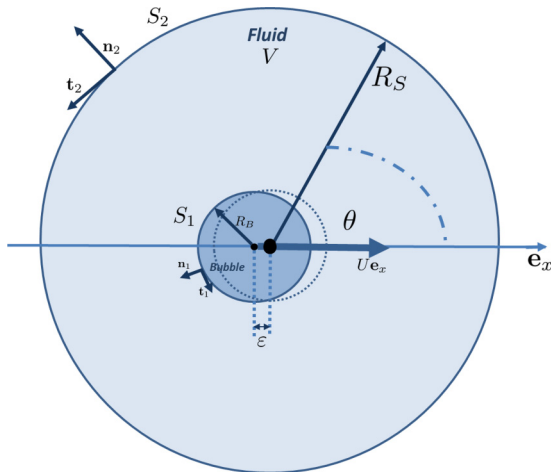

FIG. 13. Schematic of the cell model used for the drag derivation. A bubble of radius R_B with surface S_1 is surrounded by fluid of volume V with surface S_2 and radius R_S. $\mathbf{n}_1$ is a normal to S_1, $\mathbf{n}_2$ is a normal to S_2, $\mathbf{t}_1^{(\alpha)}$ are unit vectors on S_1, and $\mathbf{t}_2^{(\alpha)}$ are unit vectors on S_2. $\{\mathbf{n}_1, \mathbf{t}_1^{(1)}, \mathbf{t}_1^{(2)}\}$ and $\{\mathbf{n}_2, \mathbf{t}_2^{(1)}, \mathbf{t}_2^{(2)}\}$ are orthogonal. The bubble with the changing radius R_B is moving with velocity U along $\mathbf{e}_x$. ε is the distance between the bubble center and the center of the outer fluid sphere.

and translationally moving inside a fluid volume that was also bounded by a sphere with surface S_2. In the following, $\mathbf{n}_1$ is the normal to S_1; $\mathbf{n}_2$ is the normal to S_2; $\mathbf{t}_1^{(\alpha)}$ and $\mathbf{t}_2^{(\alpha)}$ are the unit vectors on spheres, respectively; $\mathbf{u}$ is the velocity of an inertial reference frame; and $\mathbf{v}$ is the velocity of a noninertial reference frame (bubble) that is moving with velocity $U\mathbf{e}_x$ relative to inertial frame ($\mathbf{u} = U\mathbf{e}_x + \mathbf{v}$). The following boundary conditions are applied: $q_1 = \mathbf{n}_1 \cdot \mathbf{v}$ on surface S_1 and $q_2 = \mathbf{n}_2 \cdot \mathbf{u}$ on S_2. p is the irrotational flow pressure (simulated by irrotational Bernoulli equation); τ is the stress; E is the kinetic energy; and $\mathbf{D} = \frac{1}{2}(\nabla\mathbf{u} + \nabla\mathbf{u}^T)$ is the strain rate tensor. A dissipation approximation was performed for potential flow: $\mathbf{u} = \nabla\phi$, where ϕ is the velocity potential. The boundary conditions at the surfaces of the spheres were $(\mathbf{n}_1 \cdot (-p\mathbf{I} + \tau) \cdot \mathbf{t}_1^{(\alpha)})|_{S_1} = 0$ (clean gas-liquid interface) and $[\mathbf{n}_2 \cdot (-p\mathbf{I} + \tau) \cdot \mathbf{t}_2^{(\alpha)}]|_{S_2} = 0$ (the outer boundary is a free surface). Operation : is a double dot product. For matrix A, it is defined as follows: $A : A = A_{ij}A_{ij}$.

Using the dissipation method and assumption of zero tangential stress on the outer boundary S_2, the following equation for the drag on the bubble was obtained in Ref. [56]

$$
F_D = \frac{1}{U}\left(\frac{dE}{dt} + \int_V \tau : \mathbf{D}dV - W\right), \tag{B1}
$$

where

$$
W = -\int_{S_1} \mathbf{n}_1 \cdot (-p\mathbf{I} + \tau) \cdot \mathbf{n}_1(\mathbf{n}_1 \cdot \mathbf{v})dS
$$

$$
+ \int_{S_2} \mathbf{n}_2 \cdot (-p\mathbf{I} + \tau) \cdot \mathbf{n}_2(\mathbf{n}_2 \cdot \mathbf{u})dS. \tag{B2}
$$

An approach presented in Refs. [40,87] is followed. A relation for the stress $\tau = 2\int_{-\infty}^{t} E(t-t_1)\mathbf{D}[u(\chi,t_1)]dt_1$ is considered, where χ is the path line, $\chi = \mathbf{x} - \mathbf{e}_x \int_{\tau}^{t} U(t_1)dt_1$. With the equation $\mathbf{D}[u(\chi,t_1)] = \frac{U(t_1)}{U(t)}\mathbf{D}[u(x,t)]$, stress can be written as follows:

$$\tau = \frac{2\mathbf{D}[u(x,t)]}{U(t)} \int_{-\infty}^{t} E(t-t_1)U(t_1)dt_1. \tag{B3}$$

For the derivation, denote the integral in Eq. (B3) as $I_{\text{ve}}(t) = \int_{-\infty}^{t} E(t-t_1)U(t_1)dt_1$.

Substitution of the stress from Eq. (B3) into Eq. (B1) leads to

$$F_D = \frac{1}{U}\left\{ \frac{dE}{dt} + \int_{S_1} \mathbf{n}_1 \cdot p\mathbf{I} \cdot \mathbf{n}_1(\mathbf{n}_1 \cdot \mathbf{v})dS - \int_{S_2} \mathbf{n}_2 \cdot p\mathbf{I} \cdot \mathbf{n}_2(\mathbf{n}_2 \cdot \mathbf{u})dS + \frac{2I_{\text{ve}}(t)}{U(t)} \right.$$
$$\left. \times \left[\int_{V} \mathbf{D}:\mathbf{D}dV + \int_{S_1} \mathbf{n}_1 \cdot \mathbf{D} \cdot \mathbf{n}_1(\mathbf{n}_1 \cdot \mathbf{v})dS - \int_{S_2} \mathbf{n}_2 \cdot \mathbf{D} \cdot \mathbf{n}_2(\mathbf{n}_2 \cdot \mathbf{u})dS \right] \right\}. \tag{B4}$$

The calculation of the kinetic energy rate $\frac{dE}{dt}$ from the irrotational Bernoulli equation and the Navier-Stokes incompressible equation can be found in Ref. [56]. After some algebra, Eq. (B4) yields the following expression for the drag on the bubble:

$$F_D = \int_{S_1} p\mathbf{n}_1 \cdot \mathbf{e}_x dS + \frac{2I_{\text{ve}}(t)}{U(t)}\left[-\int_{S_1}(\mathbf{n}_1 \cdot \mathbf{D} \cdot \mathbf{n}_1)\mathbf{n}_1 \cdot \mathbf{e}_x dS - \frac{1}{U}\int_{S_1} \mathbf{n}_1 \cdot \mathbf{D} \cdot \mathbf{t}_1^{(\alpha)}(\mathbf{t}_1^{(\alpha)} \cdot \mathbf{u})dS + \frac{1}{U}\int_{S_2} \mathbf{n}_2 \cdot \mathbf{D} \cdot \mathbf{t}_2^{(\alpha)}(\mathbf{t}_2^{(\alpha)} \cdot \mathbf{u})dS \right]. \tag{B5}$$

In the cell system described above, let R_B be the radius of the bubble, R_s be the radius of the surrounding liquid volume, and ε be the distance between the bubble center and center of the outer sphere. In that notation, the translational velocity of the bubble will be $U = \dot{\varepsilon}$. Later, the spherical coordinates (r, θ, φ) will be used. However, the motion is assumed to occur only in a polar plane (r, θ) (the bubble is moving only along one direction, Fig. 13).

Drag equation (B5) can be written as

$$F_D = 2\pi R_B^2 \int_0^{\pi}(p)\cos(\theta)\sin(\theta)d\theta + \frac{2I_{\text{ve}}(t)}{U(t)}\left[-2\pi R_B^2 \int_0^{\pi} D_{rr}\Big|_{R_B}\cos(\theta)\sin(\theta)d\theta \right.$$
$$\left. - \frac{2\pi R_B^2}{U}\int_0^{\pi} D_{r\theta}u_\theta\Big|_{R_B}\sin(\theta)d\theta + \frac{2\pi R_S^2}{U}\int_0^{\pi} D_{r\theta}u_\theta\Big|_{R_S}\sin(\theta)d\theta \right]. \tag{B6}$$

The following form of the velocity potential is employed [56]:

$$\phi(r,\theta,\varphi) = \frac{B_0}{r} + \left(rA_1 + \frac{1}{r^2}B_1\right)\cos(\theta), \quad A_1 = -\frac{R_B^3\left(U + 2\varepsilon\dot{R}_B R_B^{-1}\right)}{R_S^3 - R_B^3},$$

$$B_1 = -\frac{R_B^3 R_S^3\left(U + 2\varepsilon\dot{R}_B R_B^{-1}\right)}{2\left(R_S^3 - R_B^3\right)}, \quad B_0 = -R_B^2\dot{R}_B. \tag{B7}$$

Equation (B7) with $R_S \to \infty$ (infinite outer sphere), $\varepsilon \to 0$ (two spheres are concentric), and $l = 1$ can be reduced to

$$\phi(r,\theta,\varphi) = \frac{B_0}{r} - \frac{1}{r^2}\frac{R_B^3 U}{2}\cos(\theta), \tag{B8}$$

where the first term is a purely radial solution of the continuity equation (that was mentioned in Sec. II B, [32]) that corresponds to the external flow generated by bubble oscillations [88]. The second term is equal to the traditional velocity potential for a spherical bubble moving with velocity U [89].

From Eq. (B7), velocity components can be calculated as follows:

$$u_r = \frac{\partial\phi}{\partial r} = -\frac{B_0}{r^2} + \left(A_1 - \frac{2B_1}{r^3}\right)\cos(\theta), \quad u_\theta = \frac{1}{r}\frac{\partial\phi}{\partial\theta} = -\left(A_1 + \frac{B_1}{r^3}\right)\sin(\theta), \quad u_\varphi = 0. \tag{B9}$$

Now, one can calculate the strain rate tensor $\mathbf{D}$:

$$\mathbf{D} = \begin{pmatrix} \frac{2B_0}{r^3} + \frac{6B_1}{r^4}\cos(\theta) & \frac{3B_1}{r^4}\sin(\theta) & 0 \\ \frac{3B_1}{r^4}\sin(\theta) & -\frac{3B_1}{r^4}\cos(\theta) - \frac{B_0}{r^3} & 0 \\ 0 & 0 & -\frac{3B_1}{r^4}\cos(\theta) - \frac{B_0}{r^3} \end{pmatrix}. \tag{B10}$$

Then, Eq. (B6) can be calculated using Eq. (B10) for the strain rate tensor.

With $R_S \to \infty$, one can obtain the following expression from Eqs. (B6) and (B10):

$$F_D = \frac{2\pi}{3}\rho R_B^3\dot{U} + 2\pi\rho U\dot{R}_B R_B^2 + 12\pi R_B \int_{-\infty}^{t} E(t-t_1)U(t_1)dt_1. \tag{B11}$$

APPENDIX C: VISCOELASTIC DRAG FOR VISCOELASTIC MODELS OF MAXWELL FAMILY

Using Eq. (12), the viscoelastic drag force can be derived as

$$
\begin{aligned}
D_{\text{ve}} &= 12\pi R \int_0^t \left[G + \frac{\mu\lambda_2}{\lambda_1}\delta(t - t_1) + \left(\frac{\mu}{\lambda_1} - \frac{\mu\lambda_2}{\lambda_1^2} - G\right)e^{-\frac{t-t_1}{\lambda_1}} \right] U(t_1)\,dt_1 \\
&= 12\pi R G [x(t) - x_0] + 12\pi R \frac{\mu\lambda_2}{\lambda_1}U(t)[2\theta(t) - 1] + 12\pi R\left(\frac{\mu}{\lambda_1} - \frac{\mu\lambda_2}{\lambda_1^2} - G\right)e^{-\frac{t}{\lambda_1}}\int_0^t e^{\frac{t_1}{\lambda_1}}U(t_1)\,dt_1.
\end{aligned}
\tag{C1}
$$

At $t = 0$, the viscoelastic drag equals zero.

Differentiation of Eq. (C1) with respect to t ($t > 0$) leads to

$$
\begin{aligned}
\frac{dD_{\text{ve}}}{dt} &= 12\pi G\dot{R}[x(t) - x_0] + 12\pi G R U(t) + 12\pi\dot{R}\frac{\mu\lambda_2}{\lambda_1}U(t) + 12\pi R\frac{\mu\lambda_2}{\lambda_1}U_t' + 12\pi\dot{R}\left(\frac{\mu}{\lambda_1} - \frac{\mu\lambda_2}{\lambda_1^2} - G\right)e^{-\frac{t}{\lambda_1}}\int_0^t e^{\frac{t_1}{\lambda_1}}U(t_1)\,dt_1 \\
&\quad + 12\pi R\left(\frac{\mu}{\lambda_1} - \frac{\mu\lambda_2}{\lambda_1^2} - G\right)\left(-\frac{1}{\lambda_1}\right)e^{-\frac{t}{\lambda_1}}\int_0^t e^{\frac{t_1}{\lambda_1}}U(t_1)\,dt_1 + 12\pi R\left(\frac{\mu}{\lambda_1} - \frac{\mu\lambda_2}{\lambda_1^2} - G\right)U(t) \\
&= 12\pi\dot{R}\left\{ G[x(t) - x_0] + \frac{\mu\lambda_2}{\lambda_1}U(t) + \left(\frac{\mu}{\lambda_1} - \frac{\mu\lambda_2}{\lambda_1^2} - G\right)e^{-\frac{t}{\lambda_1}}\int_{-\infty}^t e^{\frac{t_1}{\lambda_1}}U(t_1)\,dt_1 \right\} \\
&\quad + \left[12\pi G R U(t) + 12\pi R\frac{\mu\lambda_2}{\lambda_1}U_t' + 12\pi R\left(\frac{\mu}{\lambda_1} - \frac{\mu\lambda_2}{\lambda_1^2} - G\right)U(t) \right] \\
&\quad + 12\pi R\left(\frac{\mu}{\lambda_1} - \frac{\mu\lambda_2}{\lambda_1^2} - G\right)\left(-\frac{1}{\lambda_1}\right)e^{-\frac{t}{\lambda_1}}\int_0^t e^{\frac{t_1}{\lambda_1}}U(t_1)\,dt_1 \\
&= \frac{\dot{R}}{R}D_{\text{ve}} + \left\{ -\frac{1}{\lambda_1}D_{\text{ve}} + \frac{12}{\lambda_1}\pi R G[x(t) - x_0] + \frac{12}{\lambda_1}\pi R\frac{\mu\lambda_2}{\lambda_1}U(t) \right\} + \left[12\pi R\frac{\mu\lambda_2}{\lambda_1}U_t' + 12\pi R\left(\frac{\mu}{\lambda_1} - \frac{\mu\lambda_2}{\lambda_1^2}\right)U(t) \right] \\
&= D_{\text{ve}}\left(\frac{\dot{R}}{R} - \frac{1}{\lambda_1}\right) + \frac{12}{\lambda_1}\pi R G[x(t) - x_0] + 12\pi R\frac{\mu}{\lambda_1}U(t) + 12\pi R\frac{\mu\lambda_2}{\lambda_1}U_t'.
\end{aligned}
\tag{C2}
$$

Equation (C2) can be written as

$$
\dot{D}_{\text{ve}} + \left(\frac{1}{\lambda_1} - \frac{\dot{R}}{R}\right)D_{\text{ve}} = 12\pi R\left\{ \frac{G}{\lambda_1}[x(t) - x_0] + \frac{\mu}{\lambda_1}U(t) + \frac{\mu\lambda_2}{\lambda_1}U_t' \right\}.
\tag{C3}
$$

[1] D. Cosgrove, Eur. J. Radiol. **60**, 324 (2006).
[2] R. Schlief, Curr. Opin. Radiol. **3**, 198 (1991).
[3] C. C. Coussios and R. A. Roy, Annu. Rev. Fluid Mech. **40**, 395 (2008).
[4] M. A. Solovchuk, S. C. Hwang, H. Chang, M. Thiriet, and T. W. H. Sheu, Med. Phys. **41**, 052903 (2014).
[5] A. J. Coleman, J. E. Saunders, L. A. Crum, and M. Dyson, Ultrasound Med. Biol. **13**, 69 (1987).
[6] C. C. Church, J. Acoust. Soc. Am. **86**, 215 (1989).
[7] Z. Xu, J. B. Fowlkes, E. D. Rothman, A. M. Levin, and C. A. Cain, J. Acoust. Soc. Am. **117**, 424 (2005).
[8] A. D. Maxwell, C. A. Cain, A. P. Duryea, L. Yuan, H. S. Gurm, and Z. Xu, Ultrasound Med. Biol. **35**, 1982 (2009).
[9] E. Brujan, *Cavitation in Non-Newtonian Fluids: With Biomedical and Bioengineering Applications* (Springer Science & Business Media, Berlin, 2010).
[10] Y.-F. Zhou, World J. Clin. Oncol. **2**, 8 (2011).
[11] T. Leslie and J. Kennedy, Int. J. Hyperthermia **23**, 173 (2007).
[12] A. Raisinghani and A. N. DeMaria, Am. J. Cardiol. **90**, 3 (2002).
[13] M. Meza, Y. Greener, R. Hunt, B. Perry, S. Revall, W. Barbee, J. P. Murgo, and J. Cheirif, Am. Heart J. **132**, 871 (1996).
[14] E. C. Unger, E. Hersh, M. Vannan, and T. McCreery, Echocardiography **18**, 355 (2001).
[15] K. Ferrara, R. Pollard, and M. Borden, Annu. Rev. Biomed. Eng. **9**, 415 (2007).
[16] R. V. Shohet, S. Chen, Y.-T. Zhou, Z. Wang, R. S. Meidell, R. H. Unger, and P. A. Grayburn, Circulation **101**, 2554 (2000).
[17] A. Lawrie, A. Brisken, S. Francis, D. Cumberland, D. Crossman, and C. Newman, Gene Therapy **7**, 2023 (2000).
[18] E. C. Everbach and C. W. Francis, Ultrasound Med. Biol. **26**, 1153 (2000).
[19] J. F. Polak, New Engl. J. Med. **351**, 2154 (2004).
[20] S. Lea, G. Price, and A. Walmsley, Ultrason. Sonochem. **12**, 233 (2005).
[21] B. Felver, D. C. King, S. C. Lea, G. J. Price, and A. D. Walmsley, Ultrason. Sonochem. **16**, 692 (2009).
[22] J. Zacharias, J. Cataract Refractive Surg. **34**, 846 (2008).
[23] A. A. Doinikov, Phys. Rev. E **64**, 026301 (2001).
[24] A. A. Doinikov, J. Acoust. Soc. Am. **116**, 821 (2004).
[25] A. A. Doinikov, Bubble Part. Dyn. Acoust. Fields **661**, 95 (2005).
[26] A. A. Doinikov and P. A. Dayton, J. Acoust. Soc. Am. **121**, 3331 (2007).

[27] L. A. Kuznetsova, S. Khanna, N. N. Amso, W. T. Coakley, and A. A. Doinikov, J. Acoust. Soc. Am. **117**, 104 (2005).

[28] R. Mettin, C.-D. Ohl, and W. Lauterborn, in *Sonochemistry and Sonoluminescence* (Springer, Berlin, 1999), pp. 139–144.

[29] R. Mettin, S. Luther, C.-D. Ohl, and W. Lauterborn, Ultrason. Sonochem. **6**, 25 (1999).

[30] R. Mettin, I. Akhatov, U. Parlitz, C. D. Ohl, and W. Lauterborn, Phys. Rev. E **56**, 2924 (1997).

[31] J. Appel, P. Koch, R. Mettin, D. Krefting, and W. Lauterborn, Ultrason. Sonochem. **11**, 39 (2004).

[32] X. Yang and C. C. Church, J. Acoust. Soc. Am. **118**, 3595 (2005).

[33] M. Warnez and E. Johnsen, Phys. Fluids **27**, 063103 (2015).

[34] E. Zilonova, M. Solovchuk, and T. Sheu, Ultrason. Sonochem. **40**, 900 (2018).

[35] C. Hua and E. Johnsen, Phys. Fluids **25**, 083101 (2013).

[36] R. Gaudron, M. Warnez, and E. Johnsen, J. Fluid Mech. **766**, 54 (2015).

[37] E. Zilonova, M. Solovchuk, and T. Sheu, Ultrason. Sonochem. (2018).

[38] F. R. Gilmore, The growth or collapse of a spherical bubble in a viscous compressible fluid, Hydrodynamics laboratory, California Institute of Technology, Pasadena, California, Report No. 26–4, 1952.

[39] V. G. Levich, *Physicochemical Hydrodynamics* (Prentice Hall, Upper Saddle River, NJ, 1962).

[40] D. D. Joseph and T. Y. Liao, J. Fluid Mech. **265**, 1 (1994).

[41] R. Löfstedt, B. P. Barber, and S. J. Putterman, Phys. Fluids A: Fluid Dynam. **5**, 2911 (1993).

[42] B. P. Barber, R. A. Hiller, R. Löfstedt, S. J. Putterman, and K. R. Weninger, Phys. Rep. **281**, 65 (1997).

[43] C. Barajas and E. Johnsen, J. Acoust. Soc. Am. **141**, 908 (2017).

[44] C. C. Coussios, C. H. Farny, G. Ter Haar, and R. A. Roy, Int. J. Hyperthermia **23**, 105 (2007).

[45] F. Chavrier, J. Chapelon, A. Gelet, and D. Cathignol, J. Acoust. Soc. Am. **108**, 432 (2000).

[46] M. Solovchuk, T. W. Sheu, and M. Thiriet, J. Acoust. Soc. Am. **134**, 3931 (2013).

[47] M. Solovchuk, T. W.-H. Sheu, and M. Thiriet, Commun. Comput. Phys. **18**, 1050 (2015).

[48] H. Z. Li, Y. Mouline, and N. Midoux, Chem. Eng. Sci. **57**, 339 (2002).

[49] A. Premlata, M. K. Tripathi, B. Karri, and K. C. Sahu, Phys. Fluids **29**, 033103 (2017).

[50] A. Premlata, M. K. Tripathi, B. Karri, and K. C. Sahu, J. Non-Newtonian Fluid Mech. **239**, 53 (2017).

[51] J. S. Allen and R. A. Roy, J. Acoust. Soc. Am. **107**, 3167 (2000).

[52] T. Watanabe and Y. Kukita, Phys. Fluids A: Fluid Dynam. **5**, 2682 (1993).

[53] M. Manjare, B. Yang, and Y.-P. Zhao, Phys. Rev. Lett. **109**, 128305 (2012).

[54] A. A. Doinikov, J. Fluid Mech. **501**, 1 (2004).

[55] S. Gavrilyuk and V. Teshukov, Eur. J. Mech. B Fluids **24**, 468 (2005).

[56] J. C. P. Inciarte, Topics in viscous potential flow of two-phase systems, Thesis, University of Minnesota (unpublished).

[57] J. Magnaudet and D. Legendre, Phys. Fluids **10**, 550 (1998).

[58] J. Sherwood, Int. J. Multiphase Flow **25**, 705 (1999).

[59] C. Ohl, A. Tijink, and A. Prosperetti, J. Fluid Mech. **482**, 271 (2003).

[60] H. L. Dryden, *Hydrodynamics* (Dover Publications, Mineola, NY, 1956).

[61] D. Moore, J. Fluid Mech. **6**, 113 (1959).

[62] J. R. Dormand and P. J. Prince, J. Comput. Appl. Math. **6**, 19 (1980).

[63] M. A. Solovchuk, T. W. Sheu, M. Thiriet, and W.-L. Lin, Appl. Therm. Eng. **56**, 62 (2013).

[64] F. A. Duck, *Physical Properties of Tissues: A Comprehensive Reference Book* (Academic Press, San Diego, CA, 2013).

[65] E. Vlaisavljevich, K.-W. Lin, A. Maxwell, M. T. Warnez, L. Mancia, R. Singh, A. J. Putnam, B. Fowlkes, E. Johnsen, C. Cain *et al.*, Ultrasound Med. Biol. **41**, 1651 (2015).

[66] E. L. Madsen, H. J. Sathoff, and J. A. Zagzebski, J. Acoust. Soc. Am. **74**, 1346 (1983).

[67] P. N. Wells and H.-D. Liang, J. R. Soc., Interface **8**, 1521 (2011).

[68] R. G. Holt and R. A. Roy, Ultrasound Med. Biol. **27**, 1399 (2001).

[69] A. Prosperetti, L. A. Crum, and K. W. Commander, J. Acoust. Soc. Am. **83**, 502 (1988).

[70] P. Marmottant, S. van der Meer, M. Emmer, M. Versluis, N. de Jong, S. Hilgenfeldt, and D. Lohse, J. Acoust. Soc. Am. **118**, 3499 (2005).

[71] J. B. Estrada, C. Barajas, D. L. Henann, E. Johnsen, and C. Franck, J. Mech. Phys. Solids **112**, 291 (2018).

[72] C. C. Church and X. Yang, J. Acoust. Soc. Am. **117**, 2530 (2005).

[73] V. Bjerknes, *Fields of Force* (General Books, Memphis, TN, 1906).

[74] N. A. Pelekasis and J. A. Tsamopoulos, J. Fluid Mech. **254**, 467 (1993).

[75] M. Minnaert, London, Edinburgh, Dublin Philos. Mag. J. Sci. **16**, 235 (1933).

[76] T. G. Leighton, *The Acoustic Bubble* (Academic, London 1994).

[77] A. Harkin, T. J. Kaper, and A. Nadim, J. Fluid Mech. **445**, 377 (2001).

[78] M. Ida, Phys. Rev. E **67**, 056617 (2003).

[79] H. N. Oguz and A. Prosperetti, J. Fluid Mech. **218**, 143 (1990).

[80] E. Zabolotskaya, Sov. Phys. Acoust. U.S.S.R. **30**, 365 (1984).

[81] A. Doinikov and S. Zavtrak, Phys. Fluids **7**, 1923 (1995).

[82] T. Barbat, N. Ashgriz, and C.-S. Liu, J. Fluid Mech. **389**, 137 (1999).

[83] A. A. Doinikov, Phys. Rev. E **59**, 3016 (1999).

[84] A. Shima, J. Basic Eng. **93**, 426 (1971).

[85] F. Mainardi and G. Spada, Eur. Phys. J.: Spec. Top. **193**, 133 (2011).

[86] D. D. Joseph, *Fluid Dynamics of Viscoelastic Liquids*, Vol. 84 (Springer Science & Business Media, Berlin, 2013).

[87] D. D. Joseph and T. Y. Liao, in *Trends and Perspectives in Applied Mathematics* (Springer, Berlin, 1994), pp. 109–154.

[88] D. Léger and R. Askovic, Int. J. Nonlin. Mech. **41**, 247 (2006).

[89] G. K. Batchelor, *An Introduction to Fluid Dynamics* (Cambridge University Press, Cambridge, 2000).